



**HAL**  
open science

## **Antagonistic impacts of benthic bioturbator species: Interconnected effects on sedimentary properties, biogeochemical variables, and microbial dynamics**

Jérôme Morelle, A. Huguet, A. Richard, Anniet M. Laverman, C. Roose-Amsaleg, Edith Parlanti, Mahaut Sourzac, Valérie Mesnage, N. Lecoq, Julien Deloffre, et al.

### ► To cite this version:

Jérôme Morelle, A. Huguet, A. Richard, Anniet M. Laverman, C. Roose-Amsaleg, et al.. Antagonistic impacts of benthic bioturbator species: Interconnected effects on sedimentary properties, biogeochemical variables, and microbial dynamics. *Journal of Experimental Marine Biology and Ecology*, 2024, 573, pp.152000-152000. 10.1016/j.jembe.2024.152000 . hal-04477915

**HAL Id: hal-04477915**

**<https://hal.science/hal-04477915v1>**

Submitted on 29 May 2024

**HAL** is a multi-disciplinary open access archive for the deposit and dissemination of scientific research documents, whether they are published or not. The documents may come from teaching and research institutions in France or abroad, or from public or private research centers.

L'archive ouverte pluridisciplinaire **HAL**, est destinée au dépôt et à la diffusion de documents scientifiques de niveau recherche, publiés ou non, émanant des établissements d'enseignement et de recherche français ou étrangers, des laboratoires publics ou privés.



Distributed under a Creative Commons Attribution - NonCommercial 4.0 International License

1 **Title:** Antagonistic impacts of benthic bioturbator species: interconnected effects on sedimentary  
2 properties, biogeochemical variables, and microbial dynamics

3  
4 **Authors:** J. Morelle<sup>1,7\*</sup>, A. Huguet<sup>3</sup>, A. Richard<sup>4</sup>, A.M. Laverman<sup>2</sup>, C. Roose-Amsaleg<sup>2</sup>, E. Parlanti<sup>4</sup>, M. Sourzac<sup>4</sup>,  
5 V. Mesnage<sup>5</sup>, N. Lecoq<sup>5</sup>, J. Deloffre<sup>5</sup>, E. Viollier<sup>6</sup>, O. Maire<sup>4</sup> and F. Orvain<sup>1</sup>

6  
7 **Affiliations:**

8 <sup>1</sup> Univ. Caen, FRE 2030 BOREA, CNRS-7208, IRD-207, MNHN, Sorbonne Université, UCBN, UA. Caen, France

9 <sup>2</sup> Univ. Rennes, CNRS, ECOBIO [(Ecosystèmes, biodiversité, évolution)] - UMR 6553, Rennes, France

10 <sup>3</sup> Sorbonne Université, CNRS, EPHE, PSL, UMR 7619 METIS, Paris, France

11 <sup>4</sup> Univ. Bordeaux, CNRS, EPOC, EPHE, UMR 5805, F-33600 Pessac, France

12 <sup>5</sup> Normandie Univ, UNIROUEN, UNICAEN, CNRS, M2C, 76000 Rouen, France

13 <sup>6</sup> IPGP, Paris, France

14 <sup>7</sup> Present address: Department of Biology and CESAM – Centre for Environmental and Marine Studies, University  
15 of Aveiro, Campus de Santiago, Aveiro, 3810-193, Portugal

16 \* Corresponding author: [jerome.morelle@ua.pt](mailto:jerome.morelle@ua.pt) ; ORCID: 0000-0003-2167-818X

17  
18 **Abstract:**

19 Macrofaunal species inhabiting intertidal mudflats and performing intense bioturbation are considered as  
20 ecosystem engineers, since they profoundly influence their physical, chemical, and biological environments.  
21 Nowadays, to complete our knowledge on the effect of bioturbation processes on the surrounding environment,  
22 interdisciplinary approach is essential to unravel their complex intertwined effects on intertidal mudflats. In this  
23 study, the effects of bioturbators on sediment properties, biogeochemical variables, and microbial dynamics  
24 (microphytobenthos, bacteria and archaea) were investigated. To this end, manipulation experiments were carried  
25 out in an intertidal mudflat of the Seine Estuary (France) by revamped the abundance of the two dominant  
26 bioturbators, *Scrobicularia plana* and *Hediste diversicolor*, in winter and late summer. Results showed that the  
27 presence of *H. diversicolor* in winter had a significant effect, with a significant increase in bed level accretion and  
28 microbial nitrate reduction rates. In contrast, the presence of *S. plana* showed no significant impact on sediment  
29 properties, most likely due to a reduced bioturbating activity at low temperature. In summer, both ecosystem  
30 engineers strongly influenced their surrounding environment but with opposite effects. The intense reworking of  
31 the sediment surface by *S. plana* limited microbial growth and enhanced erosion processes. Conversely, the  
32 presence of *H. diversicolor* favoured sediment accretion and enhanced microbial growth. Overall, this  
33 interdisciplinary study confirms the importance of these two ecosystem engineers in temperate estuarine mudflats  
34 by highlighting their simultaneous and intertwined effects on the sedimentary, physicochemical, and biological  
35 features. This confirms the importance of actively considering ecosystem engineers when restoring the natural  
36 habitats of tidal flats to cope with the different vulnerability risks related to global warming (sandification of  
37 estuarine sediments, disappearance of productive mudflats, sea level rise, vulnerability to storms and erosion).

38  
39 **Keywords:** biogeochemical cycles; ecosystem engineers; microbial communities; microphytobenthos; organic  
40 matter; sediment

41 **1. Introduction**

42 Intertidal mudflats comprise a diverse range of sedimentary habitats that serve as nursery and refuge areas  
43 for various migratory and resident species, and play a crucial role in the biogeochemical processes of estuaries and  
44 coastal ecosystems (Paterson et al. 2019). In these systems, microphytobenthic biofilms (MPB) represent the main  
45 primary producer, supporting a complex trophic network where benthic invertebrates are the primary food source  
46 for valuable consumers, such as fish and shorebirds (Dauwe et al. 1998; Underwood and Kromkamp 1999).  
47 Moreover, MPB plays an essential role in biogeochemical dynamics and sediment stabilization through the  
48 secretion of extracellular polymeric substances (EPS) (Stal 2010; Hope et al. 2020).

49 The growth and productivity of MPB are influenced by various environmental factors (Underwood and  
50 Kromkamp 1999). In nutrient rich ecosystems, MPB productivity is mainly driven by the strong variation in light  
51 intensity at the sediment surface (Behrenfeld et al. 2004; Cartaxana et al. 2011) and the substantial seasonal  
52 variation in temperature impacting both MPB and biochemical reactions (Raven and Geider 1988; Davison 1991;  
53 Claquin et al. 2008). Nevertheless, nutrient concentrations at the water-sediment interface, influenced by water  
54 fluxes and organic matter (OM) mineralization through microbial respiration, continue to exert a discernible  
55 influence on MPB (Aller and Cochran 2019), along with salinity, pH, oxygen levels, currents, and sediment  
56 properties (Underwood and Kromkamp 1999; Juneau et al. 2015; Redzuan and Underwood 2021). Finally,  
57 biological disturbances of the sediment-water interface (i.e. especially through macrofaunal bioturbation) may lead  
58 to drastic changing in sediment abiotic conditions, and thus indirectly influence MPB biomass and productivity,  
59 with far-reaching consequences for the intricate trophic network through bottom-up ecological cascades.

60 Bioturbation by macrofaunal species includes sediment reworking (mixing sediment particles) and  
61 bioirrigation (transport of solutes) processes, which are mainly related to behaviours burrowing, locomotion, and  
62 feeding activities (Kristensen et al. 2012). The impacts of macrofaunal activities on the MPB and its surrounding  
63 environment are linked to both direct (trophic) and indirect interactions (Jones et al. 1994; Bruno and Bertness  
64 2001; Crain and Bertness 2006; Ubertini et al. 2012; Van De Koppel et al. 2015). Despite the negative effects of  
65 macrofaunal bioturbation related to grazing and sediment surface disruption, bioturbating macrofauna has also  
66 been shown to positively influence microbial processes (Swanberg 1991; Orvain et al. 2004; Chennu et al. 2015,  
67 2017; Eriksson et al. 2017; D'Hondt et al. 2018). Therefore, by facilitating oxygen and solute exchange at the  
68 sediment-water interface, bioturbation activities enhance the influx of dissolved OM (DOM), aerobic OM  
69 remineralization, and nutrient cycling. Bioturbation also promotes bacterial growth by accelerating solute and  
70 particulate exchanges at the water-sediment interface, (Aller 1988; Boudreau and Jorgensen 2001; He et al. 2019).  
71 Oxygenation and sediment surface irrigation by bioturbation may also modify the redox boundary, thus influencing  
72 the quantity and quality of sedimentary OM (Fanjul et al. 2015). This, in turn, can be influenced by the structure,  
73 metabolic rate, and functioning of benthic communities (Dauwe et al. 1998; Oleszczuk et al. 2019). The chemical  
74 composition and dynamics of sedimentary and dissolved OM are thus impacted, especially because the properties  
75 of pore-water DOM produced during biodegradation processes have been shown to be mainly dependent on  
76 sedimentary OM sources (Burdige and Komada 2015; Derrien et al. 2019). Overall, the influence of bioturbation  
77 on the surrounding environment is significant, regulating sediment dynamics, bed erodibility, and biogeochemical  
78 processes, with both positive and negative effects on the microbial compartment. Some macrofauna species with  
79 high bioirrigation activity can be particularly influential, especially in cohesive sediments, where solute diffusion  
80 is limited. These positive and negative effects are expected to exhibit temporal variability as macrofaunal

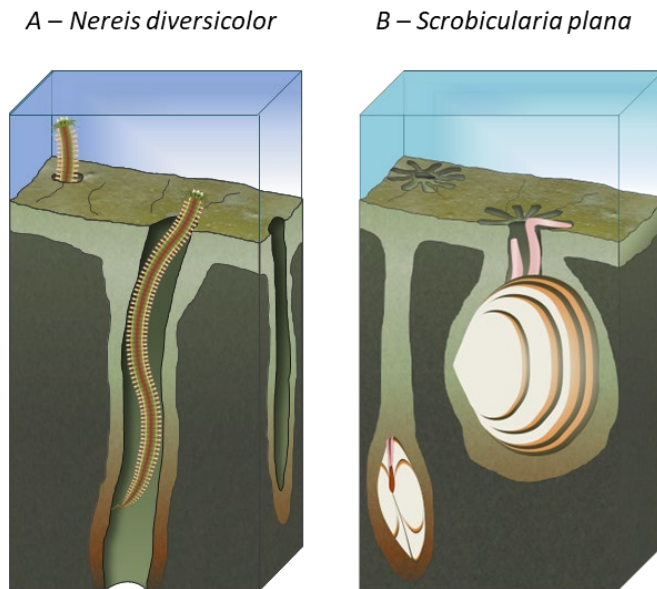
81 bioturbation has been shown to be modulated by temperature, with more pronounced effects in spring, summer,  
82 and early autumn (Admiraal and Peletier 1980; Colijn and Dijkema 1981; Underwood 1994; Stal and de Brouwer  
83 2003; Orvain et al. 2014; Cozzoli et al. 2018).

84 The impacts of benthic macrofaunal bioturbation and its regulatory effects on various properties of the  
85 surrounding environment (e.g., sediment composition, OM, nutrient recycling, recruitment of macrofaunal spats,  
86 bacterial and MPB growth, or consumption rates) have been extensively studied. However, complex interactions  
87 among all physicochemical and biological components give rise to intricate "bottom-up" and "top-down" forces  
88 that are not yet fully understood. Understanding these interactions is essential for maintaining the balance and  
89 value of the ecosystem services they provide in intertidal mudflats. Bioturbation by benthic macrofauna and its  
90 effects, which are vital drivers of mudflat structure and function, are critical elements to be considered in ecological  
91 studies and environmental management strategies. Given the findings of previous studies, it is crucial to investigate  
92 the synergistic effects. To achieve this goal, interdisciplinary studies offer a holistic and comprehensive approach  
93 that provides insights into the complex and interconnected relationships within trophic networks.

94 In this context, the present study aimed to investigate the effects of two dominant benthic macrofaunal  
95 species in intertidal mudflats on different components of the surrounding environment, including bed topography,  
96 sediment composition, biogeochemical processes, and microbial and MPB activities. The selected representative  
97 site is a temperate intertidal mudflat located downstream the Seine Estuary (northwest France). The selected  
98 ecosystem engineers (fig. 1) were the bivalve *Scrobicularia plana*, which is predominantly responsible for surface  
99 sediment reworking (Zwarts et al. 1994; Orvain 2005), and the annelid *Hediste diversicolor*, which is primarily  
100 involved in gallery bioirrigation (François et al. 2002; Passarelli et al. 2012; Richard et al. 2023). *S. plana* is a  
101 widely distributed filter feeder characterized by long siphons that enable it to bury itself in sand or mud. This  
102 species thrives at high densities along coastlines and estuaries in northern Europe, the Mediterranean, and West  
103 Africa (Santos et al. 2011). *H. diversicolor* is a versatile predator that forms distinctive U-shaped burrows in sand  
104 and mud, featuring a mucus net at the entrance. This species creates a water current within its tube to draw particles  
105 through the net. Native to the northeast Atlantic, *H. diversicolor* range extends from the Baltic Sea to the  
106 Mediterranean and has been introduced to the northwest Atlantic (Einfeldt et al. 2014).

107 Although field observations are typically conducted to study various components of a trophic network  
108 simultaneously (Weerman et al. 2011), autocorrelation and confounding factors can complicate the mechanistic  
109 understanding of intertwined processes. Therefore, field studies with addition of macrofauna and manipulative  
110 experiments are relevant to assess the role of one ecological factor, among others, in bio-mediated sediments  
111 (Montserrat et al. 2009; Van Colen et al. 2010; Donadi et al. 2013). As such, a manipulative field experiment was  
112 established with enclosures buried in sediments, each containing different densities of macrofauna. Subsequently,  
113 a wide range of sedimentary, microbial, and biogeochemical parameters were concurrently measured. This study  
114 was conducted during two contrasting periods in terms of biotic and abiotic conditions: late winter (February) and  
115 late summer (September). The main hypothesis posited that the two target organisms (*H. diversicolor* and *S.*  
116 *plana*), which typically coexist in intertidal mudflats, would have antagonistic effects on bed erodibility (stabilizer  
117 vs. destabilizer) and sediment mixing in superficial layers (dissolved exchanges vs. particulate exchanges). The  
118 positive influence of the presence of *H. diversicolor* on MPB growth was anticipated because of its impact on  
119 sediment stability and bioirrigation activities within its galleries (Morelle et al. 2021; Richard et al. 2023).  
120 Conversely, it was expected that the presence of *S. plana* would limit MPB growth owing to disruption of the

121 sediment surface (Richard et al. 2023). Furthermore, the OM quality and quantity are expected to be modified in  
122 the presence of ecosystem engineers, particularly in the dissolved phase (DOM), owing to enhanced oxygenation  
123 and sediment surface irrigation through bioturbation, especially in the presence of the gallery bioirrigator *H.*  
124 *diversicolor*.  
125



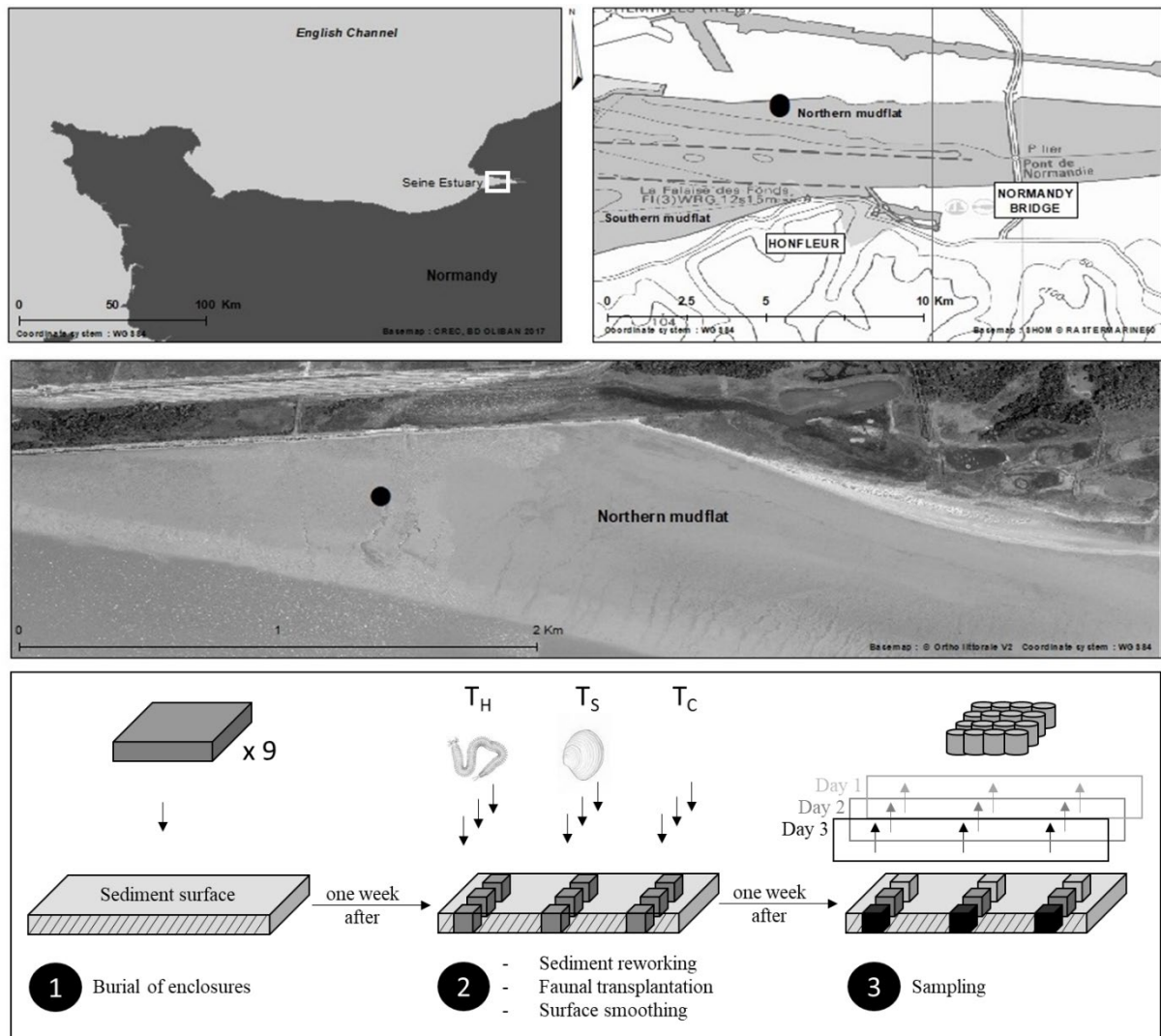
126  
127 **Figure 1. Representation of the two species studied in this work.** The annelid *Hediste diversicolor* (A) is  
128 primarily involved in gallery bioirrigation while the bivalve *Scrobicularia plana* (B) is predominantly responsible  
129 for surface sediment reworking. Copyright: illustrations from Bastien Chouquet for the MELTING POT(ES)  
130 project.

131  
132 **2. Material and Methods**

133 **2.1. Sampling site and experimental design**

134 Field experiments were conducted in the European temperate macrotidal estuary of the Seine River at an  
135 intertidal site (fig. 2). Bivalves (shell length between 40 and 43 mm) and polychaetes (body length of  
136 approximately 90 mm) were collected by hand at the same location. Specimens were stored in two distinct tanks,  
137 each approximately 100L in capacity, filled with natural seawater and sediment from the sampling site (~10 cm in  
138 depth). The water was oxygenated using air pumps, tide conditions were absent, and no supplementary food was  
139 provided. The tanks were conserved for one week in a temperature-controlled room at 12°C for winter experiment  
140 and at 21°C for late summer experiment with exposure to natural ambient light.

141



142  
 143 **Figure 2. Location of the Seine Estuary (Normandy, English Channel, France) with the sampling site located**  
 144 **in the northern mudflat (49° 27' 01.6'' N; 0° 12' 20.0''E).** The experimental design consisted in the burial of  
 145 nine enclosures. One week later, sediment inside enclosures were reworked by hand and transplanted with  
 146 macrofauna (*Hediste diversicolor*: T<sub>H</sub>; *Scrobicularia plana*: T<sub>S</sub>; and nothing for control: T<sub>C</sub>). After burial of fauna,  
 147 sediment surfaces were smoothed and one week later, several cores were sampled over 3 days from each enclosure  
 148 (1 replicate for each treatment per day: T<sub>H</sub>, T<sub>S</sub> or T<sub>C</sub>).

149  
 150 At the beginning of the experimentation, nine experimental plots (stainless steel enclosures; 50 × 50 ×  
 151 20 cm) were buried at the study site so that the top of the enclosures was precisely at the same level than the  
 152 sediment surface. To avoid additional topographical variation between replicates, enclosures were placed at a  
 153 distance of 1 m from each other in a homogeneous area of the mudflat (fig. 2). Sediment in each plot was then  
 154 gently reworked by hand up to a depth of 20 cm and the faunal enrichment was then achieved by direct addition  
 155 of the organisms in subsurface (2-3 cm) within the sediment bed. Each specimen was individually added to ensure  
 156 vitality and to accurately record the number of individuals in each replicate. In February, the enrichment  
 157 represented an addition of 35 individuals per replicate (140 ind m<sup>-2</sup>) while in September, the enrichment  
 158 represented an addition of 110 individuals (440 ind m<sup>-2</sup>). The final densities represented the maximum densities  
 159 observed at the study site during the sampling periods (comm. pers. Chloé Dancie – “Cellule de Suivi du Littoral

160 Normand | CSLN<sup>®</sup>). In order to have a net monospecific dominance for the two treatments with faunal addition,  
161 three replicates were enriched with *S. plana* (treatment T<sub>S</sub>) and three others were enriched with *H. diversicolor*  
162 (treatment T<sub>H</sub>). After animal addition, the sediment surface was flattened in all experimental units, to assess later  
163 the effects of bioturbation on bed level. Sediments in control plots were reworked by hand and flattened similarly  
164 but without faunal addition (control treatment T<sub>C</sub>). The process of the aforementioned steps was completed within  
165 one low-tide period. After one week under *in situ* conditions, the samplings were conducted during neap tides,  
166 when low-tide coincided with mid-day conditions. The different enclosures were sampled over 3 days due to tidal  
167 and safety conditions in intertidal zones. Each day, measurements were performed in successive samplings for one  
168 line of enclosure units (fig. 2), including one replicate of each treatment (T<sub>C</sub>, T<sub>H</sub>, T<sub>S</sub>) by following the same  
169 sampling method. In addition, the natural state of the mudflat sediment was also sampled each day and assigned  
170 as natural treatment (T<sub>N</sub>). The experiments were performed in the two most contrasted periods of the year in late  
171 winter (February 9<sup>th</sup> - 26<sup>th</sup>, 2018) and late summer (September 18<sup>th</sup> - October 4<sup>th</sup>, 2018). For that, enclosures were  
172 removed after the winter experiment and the whole process was repeated for the summer experiment.

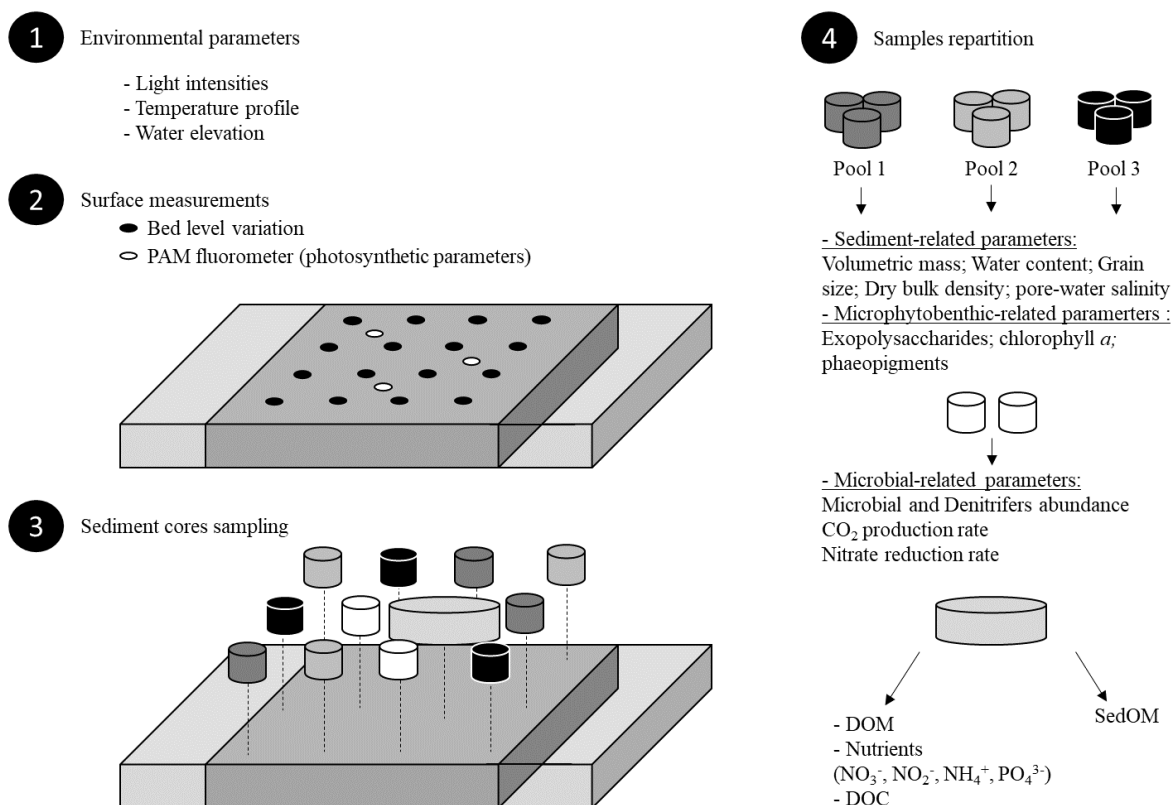
173

## 174 2.2. Sampling methods

175 The sampling protocol followed was schematically described in figure 3. Due to the interdisciplinary  
176 approach and the number of measurements requiring a relatively high quantity of sediment within each enclosure,  
177 the sampling strategy followed a precise protocol which was not random but statistically relevant (see 2.4).  
178 Throughout each manipulative experiment, environmental parameters (light intensity, temperature profile, water  
179 elevation) were recorded *in situ* at the study site, outside the enclosures. Light intensities were recorded every 15  
180 min using an Onset Hobo UA-002 Pendant light/temperature data logger placed 15 cm above sediment surface.  
181 Vertical temperature profiles were performed every 15 min using five submersible temperature data loggers (Onset  
182 Hobo<sup>®</sup> Pendant<sup>®</sup> UA-001) placed at 0, 2, 5, 10 and 15 cm depth using a holder buried in the sediment. Water  
183 elevation was measured using a NKE<sup>©</sup> Altus based on a piezo-resistive pressure sensor (accuracy was +/-60 mm  
184 while resolution was +/- 8 mm). This instrument was set up to achieve one measurement every 30 seconds.

185 For each treatment with enclosure (T<sub>C</sub>, T<sub>H</sub>, T<sub>S</sub>), the bed level variation was estimated to evaluate the bed  
186 accretion or erosion. To this aim, a measurement of the height distance between the enclosure borders (initial  
187 sediment surface after flattening) and the sediment surface was performed by using a calliper on 16 fixed points  
188 evenly distributed over the surface with a step of 10 cm from each other (fig. 3; total surface of 0.25 m<sup>2</sup>).

189



190

191 **Figure 3. Schematic representation of the successive actions carried out during each sampling day.** The  
 192 environmental parameters (light intensities, temperature profiles and water elevation) were measured  
 193 continuously. The first measurements made were the variation of the bed level which was measured at 16 different  
 194 points and the PAM fluorometer made at 3 different positions. These two measurements did not disturb the  
 195 sediments. Then, the sediment cores were sampled, and the sediment was distributed and conditioned for future  
 196 analysis of the parameters considered in this study.

197

198 Immediately after bed level variation measurement, chlorophyll fluorescence was measured in triplicate  
 199 ( $n=3$ ) at the sediment surface within each enclosure. This was performed using a Fiber-PAM fluorometer (PAM-  
 200 control unit and WATER-EDF-universal emitter detector unit; Walz, Effeltrich, Germany) following the method  
 201 fully described in Morelle et al. (2020). Each replicate was exposed to nine actinic irradiance steps from 0 to 168  
 202  $\mu\text{mol photons m}^{-2} \text{s}^{-1}$  in winter and from 0 to 1130  $\mu\text{mol photons m}^{-2} \text{s}^{-1}$  in summer. These irradiance ranges were  
 203 chosen as they match with those of the light environment of each season (Morelle et al. 2018). The treatment of  
 204 the fluorescence data using the model of Eilers and Peeters (1988) allowed assessment of photosynthetic  
 205 parameters, i.e., the maximum effective quantum yield of the PSII ( $F_v/F_m$ ), the photosynthetic efficiency ( $\alpha$ ;  
 206 relative unit), the optimal irradiance for photosynthesis ( $E_{\text{opt}}$ ;  $\mu\text{mol photons. m}^{-2} \text{s}^{-1}$ ), the relative maximum  
 207 electron transport rate ( $r\text{ETR}_{\text{max}}$ ; relative unit), and the saturation coefficient of light ( $E_k$ ;  $\mu\text{mol photons. m}^{-2} \text{s}^{-1}$ ).

208 Afterwards, the sediment was sampled through core extraction. Two plexiglass rings (4 cm in diameter  
 209 down to a depth of 1 cm) were sampled to study the microbial activity and abundance. A fraction of 3 ml from the  
 210 first ring was stored at  $-80^\circ\text{C}$  for bacterial abundance determination. The remaining sediment from the first ring  
 211 and the second ring were kept at  $4^\circ\text{C}$  for the microbial activity experiments. Then, nine cores (2.4 cm in diameter



212 down to a depth of 1 cm) were collected and distributed into 3 pools, each representing 13.5 ml of sediment which  
213 were cautiously homogenised. For each pool, a fresh sediment aliquot (5 ml) was used for sedimentary analyses.  
214 Another sediment aliquot (5 ml) was used to determine exopolysaccharides concentrations. The last sediment  
215 aliquot (1.5 ml) was stored at -20 °C for analyses of photopigment concentrations. A last sediment core (9.3 cm in  
216 diameter down to a depth of 30 cm) was sampled to analyse the pore-water vertical profiles. Interstitial pore-water  
217 samples were extracted using Rhizon samplers (pore size 0.15 µm mean) and polypropylene syringes at a depth  
218 interval of 0 – 1 cm (for more information see Seeberg-Elverfeldt et al. (2005)). Each pore water sample was  
219 divided into two aliquots and stored in the dark at 4°C. The first aliquot of pore-water was kept for measuring  
220 nutrient (Si(OH)<sub>4</sub>, PO<sub>4</sub><sup>3-</sup>, NH<sub>4</sub><sup>+</sup>, NO<sub>2</sub><sup>-</sup>, and NO<sub>3</sub><sup>-</sup>) and dissolved organic carbon (DOC) concentrations. The second  
221 aliquot was stored for DOM spectroscopic analyses. The 0 – 1 cm depth interval of the core was then sliced and  
222 frozen at -20 °C, freeze-dried, ground, and homogenised before sedimentary organic matter (SedOM)  
223 characterization.

224

### 2.3. Analytical methods

#### 2.3.1. Sediment-related parameters.

227 To estimate the sediment-related parameters, each aliquot of sediment sampled from the pooled cores (5  
228 ml) was weighted to estimate the volumetric mass and was kept at -20°C. After freeze-drying for 24h, the water  
229 content ( $\omega$ ; %) was determined as a percentage of water relative to the total fresh weight. Subsequently, sediment  
230 was used for granulometric analysis. For that, sediments were digested in 6% hydrogen peroxide for 48 h to remove  
231 OM. The grain size distribution was then measured on subsamples using a LS Coulter particle size analyser. The  
232 mud sediment fraction was estimated as the percentage of silt particles < 63 µm (% of fine particles) and the  
233 median grain size diameter was estimated from cumulative percentage histogram. The dry bulk density ( $C_{\text{sed}}$ , kg  
234 m<sup>-3</sup>) was then estimated from  $\omega_D$  (Water weight / Dry weight × 100) and grain density ( $\gamma_s$ ; kg m<sup>-3</sup>) according to  
235 the equation  $C_{\text{sed}} = (\gamma_s \times 1000) / [(\omega_D/100) \times \gamma_s + 1000]$ .

236 Nutrients (NO<sub>3</sub><sup>-</sup>, NO<sub>2</sub><sup>-</sup>, NH<sub>4</sub><sup>+</sup>, PO<sub>4</sub><sup>3-</sup>) and DOC concentrations were obtained from the pore-water samples.  
237 Dissolved/reactive silica (Si(OH)<sub>4</sub>) concentrations were determined from filtered samples by spectrophotometry  
238 (Koroleff, (1983), silico-molybdenum blue method) using a QuAatro (Seal Analytical) continuous segmented  
239 flow analyzer. Dissolved nitrates (N-NO<sub>3</sub><sup>-</sup>) and nitrites (N-NO<sub>2</sub>) concentrations were analysed using a Gallery™  
240 Discrete Analyzer (ThermoFisher scientific, Waltham, Massachusetts, USA). The reactive phosphate P-PO<sub>4</sub><sup>3-</sup> and  
241 the dissolved ammonium N-NH<sub>4</sub><sup>+</sup> were analysed using a Technicon Auto-analyzer II, with a detection limit of 14  
242 µg L<sup>-1</sup> and 42 µg L<sup>-1</sup>, respectively for P-PO<sub>4</sub><sup>3-</sup> and N-NH<sub>4</sub><sup>+</sup> and a standard error lower than 5%. DOC was analysed  
243 using a “TOC Shimadzu 5050” carbon analyser with two injections or three if the standard error was higher than  
244 5%.

245

#### 2.3.2. Microphytobenthos-related parameters.

247 Colloidal and bound fraction of exopolysaccharides were immediately separated from the sediment  
248 aliquot (5 ml) using Dowex and conserved at -20°C for analyses following the method fully described in Morelle  
249 et al. (2020). The concentrations of high molecular weight (HMW) exopolysaccharides (after separation from  
250 Low-MW EPS in 70% Ethanol) were then measured for the colloidal (C-EPS) and bound (B-EPS) fractions.  
251 Carbohydrate contents were estimated using sulfuric acid and phenol with glucose as a standard (Dubois et al.

252 1956). Protein contents were estimated using the Bradford assay with bovine serum albumin (BSA) from Sigma-  
253 Aldrich as standard (Bradford 1976).

254 After freeze drying, photopigments were extracted from 1g of dry weight (DW) sediment in 90% acetone  
255 and the fluorescence of the supernatant was measured using a Turner Trilogy fluorometer (Turner Designs,  
256 Sunnyvale, California, USA). Chlorophyll *a* (chl *a*) and phaeopigments concentrations were calculated from the  
257 fluorescence values obtained before and after acidification following the method of Lorenzen (1967). The  
258 phaeopigment contents were expressed as a percentage of total photopigments.

259

### 260 **2.3.3. Microbial-related parameters.**

261 Microbial abundances were obtained after DNA extraction from approximately 0.5 g of fresh surface  
262 sediment (0-1 cm) according to the protocol detailed in Hellequin et al. (2018) modified from Quaiser et al. (2014).  
263 They were determined by quantitative PCR targeting generalist (*16S rRNA* genes of bacteria or archaea) and  
264 functional genes as Clade I *nosZ* gene and Clade II *nosZ* gene for N<sub>2</sub>O-reducers and calibrated with standard  
265 positive DNA. For the *16S rRNA* gene, the standard for Bacteria was DNA of *Pseudomonas fluorescens* SBW25  
266 using primers 63f and BU16S4 (Muyzer et al. 1993; Marchesi et al. 1998) and PCR fragment cloned of  
267 *Nitrososphaera viennensis* for Archaea with primers Arch806F and Arch915R (Takai and Horikoshi 2000). As in  
268 Jones et al. (2013), the standards for *nosZ* genes corresponded to PCR fragment cloned of *Bradyrhizobium*  
269 *japonicum* USDA 110 for Clade I and *Gemmatimonas aurantiaca* T-27 for Clade II. No-template controls were  
270 performed in duplicate and assays in triplicate. Amplifications were performed in a Lightcycler 480 (LC480,  
271 Roche) using Sensyfast Sybr no rox kit (Biotechnofix). Analyses were carried out with LC480 software (release  
272 1.5.1) consisting in melting curves and absolute quantification by second derivative maximum analysis method  
273 allowing the determination of the crossing points (Cp). We defined the detection limit as fluorescent signals with  
274 at least 5 Cp below the signal of the no-template controls.

275 The potential of sedimentary organic carbon degradability was determined in batch incubations by  
276 measuring the CO<sub>2</sub> production rate under anoxic conditions. To this end 5 ml of the sediment was placed in a  
277 serum bottle with 20 ml of water collected on site (filtered at 0.2 µm). The headspace was replaced by Argon to  
278 create anoxic conditions and 500 µM nitrate (NaNO<sub>3</sub>) was added. Batches were incubated at 20 °C and agitated  
279 (150 g). Samples from the headspace were analysed for CO<sub>2</sub> using a micro-GC Agilent 3000 (SRA Instrument) at  
280 the beginning of the incubation, after 2 hours and 4 hours. The CO<sub>2</sub> production was determined over the 4 hours  
281 and expressed as CO<sub>2</sub> production in gDW<sup>-1</sup> h<sup>-1</sup>.

282 The potential nitrate reduction rates were estimated from the sediment samples by performing a flow-  
283 through reactor experiment. For description of the method see (Laverman et al. 2006, 2012). The reactors were  
284 supplied with anoxic saline water (adapted to the onsite salinity) containing 5 mM of NaNO<sub>3</sub> at a flow rate of 3 ml  
285 h<sup>-1</sup> with a peristaltic pump and incubated at a constant temperature (20°C). The reactors were run for approximately  
286 30 hours, allowing determination of nitrate consumption using the *in situ* available carbon present in the sediment.  
287 NO<sub>3</sub><sup>-</sup>, NO<sub>2</sub><sup>-</sup>, NH<sub>4</sub><sup>+</sup> concentrations were determined via a Gallery (ThermoFisher) from outflow samples collected  
288 at 2-hour intervals. Samples from the input solution were also collected and analysed for the exact nitrate  
289 concentrations. Potential nitrate reduction rates were then calculated and expressed in nmol NO<sub>3</sub><sup>-</sup> per cm<sup>3</sup> of fresh  
290 sediment per hour.

291

#### 292 2.3.4. Organic matter-related parameters.

293 DOM spectroscopic analyses were performed on filtered samples. Excitation-emission matrix (EEM)  
294 fluorescence spectra were acquired, depending on the pore water volume available, in 1 or 0.5 cm path length  
295 quartz SUPRASIL® QS cuvettes (Hellma) regulated at 20 °C, using a Jobin-Yvon Fluorolog FL3-22  
296 spectrofluorometer in ratio mode with 4 nm bandwidth for both excitation (250-410 nm, 10 nm intervals) and  
297 emission (260-700 nm, 1 nm increments and 0.5 s integration time) (Parlanti et al. 2000). Samples were diluted, if  
298 necessary, to avoid inner filter effects, and their spectra, obtained by subtracting an ultrapure water (Milli-Q,  
299 Millipore) blank spectrum, were instrumentally corrected as described previously (Huguet et al. 2009). The  
300 subsequent fluorescence indices were computed to provide insights into the origin, maturity, and transformation  
301 of dissolved organic matter (DOM). The humification index (HIX), indicative of the aromaticity level and maturity  
302 of DOM (Zsolnay et al. 1999), was determined based on the position of the emission spectra. Specifically, the  
303 upper quarter area (435 - 480 nm) of the usable emission peak was divided by the lower usable quarter area  
304 (300 - 445 nm). This calculation facilitated the differentiation between strongly humified organic material,  
305 primarily of terrestrial origin ( $10 < \text{HIX} < 16$ ), and autochthonous organic material ( $\text{HIX} < 5$ ). Another key  
306 fluorescence index, the fluorescence index (FI), expressed as  $f_{450}/f_{500}$ , represents the ratio of fluorescence intensity  
307 at the emission wavelength 450 nm to that at 500 nm with an excitation wavelength of 370 nm. This index aids in  
308 discriminating between microbial ( $\text{FI} = 1.9$ ) and terrestrial sources ( $\text{FI} = 1.3$ ) of aquatic DOM (McKnight et al.  
309 2001). Additionally, the biological index (BIX), serving as a proxy for fresh autochthonous DOM production  
310 associated with biological activity (Huguet et al. 2009), was computed at an excitation wavelength of 310 nm. It  
311 involves dividing the fluorescence intensity emitted at an emission wavelength of 380 nm by that emitted at 430  
312 nm. BIX values exceeding 0.8 indicate a predominantly autochthonous origin of DOM and the presence of freshly  
313 released organic matter into the water, while lower BIX values (0.6 – 0.7) suggest moderated DOM production in  
314 natural waters.

315 The elemental (organic carbon, nitrogen) and isotopic ( $\delta^{13}\text{C}$ ) analyses of the SedOM were performed on  
316 sediment samples after being decarbonated as previously described (Thibault et al. 2019).

317 Lipid extractions were performed using on average 20 g of sediment. Samples were ultrasonically  
318 extracted at room temperature with a dichloromethane (DCM)/ methanol (MeOH) mixture (5:1) for 10 minutes (3  
319 times). Each extraction was followed by centrifugation (3500 rpm, 10 minutes) and pooling of all extracts. The  
320 total lipid extract was rotary evaporated and separated into three fractions of increasing polarity on a column of  
321 activated silica: (i) 30 ml of heptane; (ii) 30 ml of heptane:DCM (1: 4, v:v); (iii) 30 ml of DCM:MeOH (1:1, v:v).  
322 Each fraction was then rotary evaporated.

323 The *n*-alkanes, contained in the first fraction, were analysed by gas chromatography coupled to a mass  
324 spectrometer (GC–MS) using an Agilent Network 6890 GC System coupled with a 5973 Mass Selective Detector,  
325 as previously described by Coffinet et al. (2017). 1.1 µg of internal standard (*n*-tetracosane- $d_{50}$ ; Sigma-Aldrich)  
326 was added just before injection. The different *n*-alkanes were semi-quantified based on their retention time, after  
327 extraction of the characteristic  $m/z$  57 fragment.

328 The *n*-alcohols were analysed in the third fraction containing the polar compounds. Before GC-MS  
329 analysis, the fraction was dissolved in DCM and derivatized by adding 10% in volume a solution of  
330 N,O- bis(trimethylsilyl)trifluoroacetamide – Trimethylchlorosilane 99:1 (Grace Davison Discovery Science,  
331 USA). The separation was achieved with the same equipment as above. The GC oven initial temperature was set

332 to 70 °C (maintained for 1 min), increased to 130 °C at 20°C min<sup>-1</sup> and then to 320 °C at 4 °C min<sup>-1</sup> (maintained  
333 for 25 min). Samples were injected in split mode (ratio 30:1), the injector being at 280 °C. 1.5 µg of internal  
334 standard (5 $\alpha$ -cholestane; Sigma-Aldrich) was added just before injection. The silylated *n*-alcohols were semi-  
335 quantified based on their retention time, after extraction of the characteristic *m/z* 75 fragment.

336 The relative abundances of *n*-alkanes and *n*-alcohols were used to discriminate OM sources in natural  
337 environments. Thus, terrestrial vascular plants are dominated by odd long-chain *n*-alkanes (C<sub>23</sub>-C<sub>35</sub>), with C<sub>27</sub>, C<sub>29</sub>  
338 and C<sub>31</sub> being the dominant homologues (Bianchi and Canuel (2011) and references therein), and by long-chain *n*-  
339 alcohol ( $\geq$  C<sub>20</sub>) (Eglinton and Hamilton 1967). In contrast, algae and bacteria are dominated by short-chain *n*-  
340 alkanes, with C<sub>15</sub>, C<sub>17</sub>, or C<sub>19</sub> predominance, and short-chain *n*-alcohols (C<sub>12</sub>-C<sub>18</sub>). Submerged macrophytes have  
341 an intermediate composition, with a predominance of mid-chain *n*-alkanes (C<sub>21</sub>, C<sub>23</sub> or C<sub>25</sub>; Bianchi and Canuel  
342 (2011)). In the following, the relative abundance of C<sub>27</sub> + C<sub>29</sub> + C<sub>31</sub> *n*-alkanes *vs.* odd *n*-alkanes in the range C<sub>15</sub>-  
343 C<sub>31</sub> will be considered as a proxy of terrestrial OM. Similarly, the relative abundance of long-chain *n*-alcohol ( $\geq$   
344 C<sub>20</sub>) *vs.* total *n*-alcohols (i.e., short (C<sub>12-18</sub>) + long-chain homologues) will be used to estimate the proportion of  
345 terrestrial *vs.* aquatic (algal/bacterial) OM (e.g., Vonk et al. (2008)).

346

#### 347 **2.4. Statistical analyses**

348 In terms of statistical analyses, it was impossible to include the “season factor” since the fauna treatment  
349 was not the same at the two seasons. The densities were chosen to be representative of the observed maximum at  
350 each specific season in historical surveys of macrozoobenthic communities. The experiments achieved in winter  
351 end and summer end must be therefore considered as 2 independent experiments in contrasted conditions to better  
352 unravel the effect of the bioturbators on other properties.

353 For each season, all samples were taken one week after faunal treatments, in a whole 10 × 10 m square  
354 experimental study area (one per season) delimited by two perpendicular lines spaced 2 meters apart. The sampling  
355 period lasted 3 days. Each day, one replicated square of the 4 treatments was randomly chosen according to the  
356 sampling design described in a previous field study (Orvain et al. 2012, 2014), so that day effect cannot bias the  
357 analysis. In these squares, surficial sediment was systematically sampled in 1 hour at mid-tide condition to avoid  
358 any difference related to the inundation time. No difference was detected between sampling days for all variables.

359 Concerning spatial independence, a preliminary analysis of spatial autocorrelation was performed to  
360 evaluate the independence requirements on the site regarding the two main variables (i.e., sediment composition  
361 and chlorophyll content). This allowed to guarantee that the condition of spatial independence was not  
362 compromised in the analysis since, at 2 meters of distance between each subunit plot, the hypotheses of null  
363 autocorrelation was not rejected. A Durbin-Watson test allowed us to confirm the absence of spatial autocorrelation  
364 between sub-units, when applying a regression test between sediment composition and chl *a* content.

365 After that Shapiro-Wilk normality tests and Bartlett equal variance tests were applied on each parameter  
366 of the dataset, statistical analyses were performed by using a one-way ANOVA to compare the 4 treatments (T<sub>C</sub>,  
367 T<sub>H</sub>, T<sub>S</sub>, and T<sub>N</sub>) using the R software (version 4.0.2). In the case of significant differences in the ANOVA ( $p <$   
368  $.05$ ), Tukey comparison tests were performed with the considered factor to discriminate differences. The non-  
369 parametric test of Kruskal-Wallis followed by pairwise-t-tests was used when conditions were invalid. Correlations  
370 between parameters were tested using Pearson correlation tests.

371

### 372 3. Results

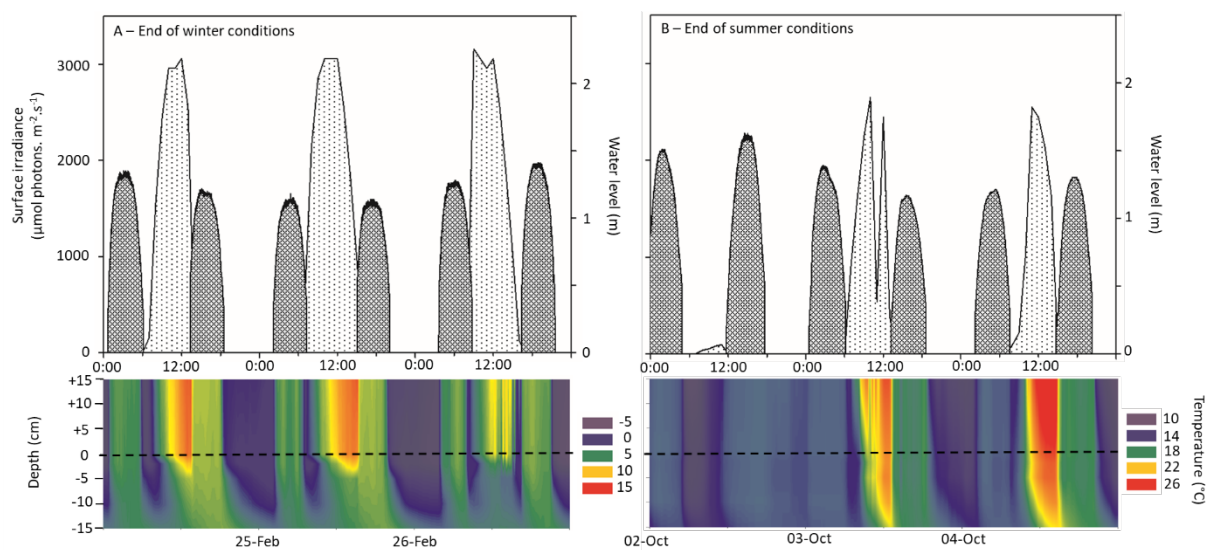
#### 373 3.1. Meteorological conditions during sampling and impact of experimental design

374 Irradiance level varied following the daily cycle with a maximum of  $3000 \mu\text{mol photons m}^{-2} \text{s}^{-1}$  for  
375 winter and  $2600 \mu\text{mol photons m}^{-2} \text{s}^{-1}$  for late summer period except during the 1<sup>st</sup> day of the survey, where  
376 irradiance values reached a maximum of  $95 \mu\text{mol photons m}^{-2} \text{s}^{-1}$  (fig. 4). During the low-tide period (lasting  
377  $\sim 5.5\text{h}$ ), the average values were  $1650 \mu\text{mol photons m}^{-2} \text{s}^{-1}$  in winter and  $657 \mu\text{mol photons m}^{-2} \text{s}^{-1}$  for late  
378 summer period.

379 A diurnal cycle was also observed for temperature values (fig. 4), which varied between  $-5.5$  and  $+13.8$   
380  $^{\circ}\text{C}$  for winter and between  $+9.7$  and  $+35.1$   $^{\circ}\text{C}$  for late summer period. Maximal values were observed during zenith,  
381 while minimal values were observed during the nocturnal low tide. During the winter sampling period, the  
382 temperature values in the sediment surface were lower than  $0^{\circ}\text{C}$ , leading to frost events. At 2 cm depth, the range  
383 of temperature variation was lower than on the surface with values between  $-1.3$  and  $+7.2$   $^{\circ}\text{C}$  for winter and  
384 between  $+11.3$  and  $+25.1$   $^{\circ}\text{C}$  for late summer period (fig. 4).

385 The impact of the deployment of experimental enclosures was estimated by considering the differences  
386 between the control treatment ( $T_C$ ) and the natural state around enclosures ( $T_N$ ). A significant difference was  
387 observed between  $T_C$  and  $T_N$  on DOM index and phaeopigments in winter (table 1). For the other parameters and  
388 in summer, it was assumed that differences between  $T_H$ ,  $T_S$ , and  $T_C$  revealed treatment-related effects and did not  
389 result from an experimental artifact.

390



391  
392 **Figure 4. Variation of environmental parameters during the monitoring periods under (A) winter and (B)**  
393 **late summer conditions.** With the depth profile of temperature in sediment ( $^{\circ}\text{C}$ ), surface irradiance ( $\mu\text{mol photons}$   
394  $\text{m}^{-2} \text{s}^{-1}$ ) in pale grey, and water level (m) in dark grey.

395

#### 396 3.2. Winter conditions

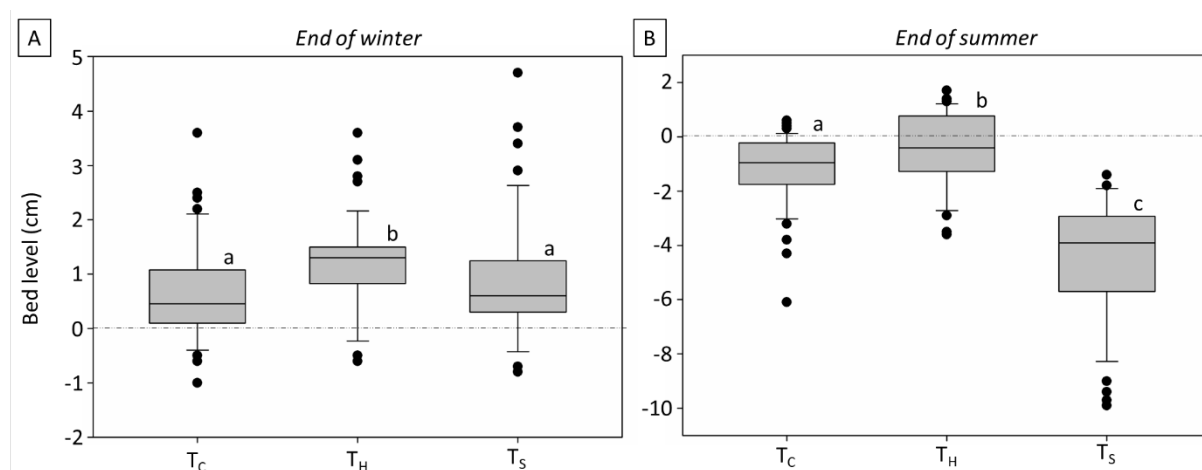
##### 397 3.2.1. Sedimentary parameters

398 In each treatment ( $T_C$ ,  $T_H$ ,  $T_S$ ), the bed level variation showed an increase in sediment height (Table 1;  
399 Figure 5-A). This sediment accumulation was significantly higher in the presence of *H. diversicolor* with  $1.2 \pm 0.6$   
400 cm compared to the control ( $0.7 \pm 0.7$  cm) or in the presence of *S. plana* ( $0.9 \pm 0.8$  cm). No other significant

401 differences were recorded between the treatments for sedimentary parameters, with an average of  $14.2 \pm 5.3\%$  fine  
 402 particles (median of  $155.7 \pm 9.8$ ), a volumetric mass of  $1.9 \pm 0.1$  kg/L, a dry bulk density of  $1633.1 \pm 47.8$  kg/m<sup>3</sup>,  
 403 and a water content of  $23.6 \pm 1.8\%$  (supp. table 1).

404 The parameters related to the SedOM also showed no differences between treatments (supp. table 1).  
 405 Total organic carbon (TOC) ranged between 0.07 and 0.37 % while total nitrogen (T<sub>N</sub>) was very low between 0.01  
 406 and 0.05%. The  $\delta^{13}\text{C}$  showed values between -24.44 to -29.44%. The relative abundance of odd long chain *n*-  
 407 alkanes vs. total odd *n*-alkanes was higher than 50 % in most of the samples (on average  $61.0 \pm 9.3\%$ ). Similarly,  
 408 long chain *n*-alcohols were largely predominant among total *n*-alcohols in all samples (on average  $86.1 \pm 5.0\%$ )  
 409 without any difference related to the treatment.

410



411 **Figure 5. Bed level variation** with averaged and quartile distribution by gathering all treatments (control: T<sub>C</sub>,  
 412 *H. diversicolor*: T<sub>H</sub>, and *S. plana*: T<sub>S</sub>) for the cold season (A) and at the end of the hot season (B). The lower-case  
 413 letters on box plot correspond to the statistical groups, the groups being separated by a significant difference after  
 414 a Tukey comparison tests.

416

417 **Table 1. Significant differences observed between the values measured in the control treatment (T<sub>C</sub>) and**  
 418 **each of the others (T<sub>N</sub>, T<sub>H</sub>, and T<sub>S</sub>) during the winter season.** With average and standard deviation values as a  
 419 function of *n* (given in the corresponding column). The stars given to values correspond to the significant  
 420 difference with T<sub>C</sub> ( $p < 0.05$ : \*;  $p < 0.01$ : \*\*;  $p < 0.001$ : \*\*\*) obtained using a Tukey comparison test or a non-  
 421 parametric pairwise t-test.

Treatment	n	T <sub>N</sub>	T <sub>C</sub>	T <sub>H</sub>	T <sub>S</sub>
Bed level (cm)	48	n.d.	+ 0.66 ± 0.67	+ <b>1.20 ± 0.58 ***</b>	+ 0.95 ± 0.83
Biological index (BIX)	3	<b>0.69 ± 0.00*</b>	0.80 ± 0.00	0.72 ± 0.03	0.74 ± 0.02
Fluorescence index (FI)	3	<b>1.25 ± 0.01***</b>	1.43 ± 0.01	<b>1.24 ± 0.01***</b>	<b>1.26 ± 0.02***</b>
Nitrate reduction rates (nmolNO <sub>3</sub> <sup>-</sup> cm <sup>-3</sup> h <sup>-1</sup> )	15	32.4 ± 8.3	32.0 ± 8.7	<b>42.6 ± 3.7 *</b>	32.9 ± 7.4
Phaeopigments (%)	9	<b>54.7 ± 5.3*</b>	45.1 ± 8.6	48.6 ± 8.5	47.7 ± 5.7
Colloidal carbohydrates EPS (µgEPS gDSW <sup>-1</sup> )	9	14.6 ± 12.7	36.9 ± 10.5	18.8 ± 9.2	<b>13.9 ± 3.9**</b>

422

### 423 3.2.2. Interstitial water parameters

424 In interstitial water samples, the DOC showed high values with on average  $7.7 \pm 1.9 \text{ mgC L}^{-1}$  (supp. table  
425 1). The DOM optical properties (illustrated from the fluorescence indices HIX, BIX and FI) highlighted a  
426 significant treatment effect for BIX and FI (table 1). The HIX index showed values lower than 5 for  $T_C$  while  
427 higher values were observed for  $T_N$ ,  $T_H$  and  $T_S$ , reaching a maximum of about 8 for  $T_S$  (supp. table 1). The BIX  
428 values ranged between 0.69 and 0.80, with significant higher values for  $T_C$  (0.8) than other treatments (0.69 for  
429  $T_N$ , 0.72 for  $T_H$  and 0.74 for  $T_S$ ). The FI index showed similar trends as the BIX, with a significant difference  
430 between  $T_C$  (1.43) and the other treatments (around 1.25). In contrast, the different nutrient concentrations in pore  
431 water showed no significant differences between treatments (supp. table 1).

432

### 433 3.2.3. Biological related parameters

434 Overall, the microbial density in the sediment (bacteria and archaea) showed low values with no  
435 significant differences between treatment (on average  $22.7 \times 10^4 \pm 9.7 \times 10^4$  microbial (*16S rRNA*) gene copy  
436 number per ng of extracted DNA; supp. table 1). Archaea made up 40.5 % of this total microbial community.  
437 Despite the differences observed in optical DOM properties, the microbial degradation activity illustrated through  
438 the  $\text{CO}_2$  production rate showed no differences between treatments with on average  $73.3 \pm 10.8 \text{ nmol CO}_2 \text{ gDSW}^{-1} \text{ h}^{-1}$ .  
439 In contrast, the potential nitrate reduction rates showed significantly higher values in presence of *H.*  
440 *diversicolor* than in other treatments (on average  $42.6 \pm 3.7 \text{ nmol cm}^{-3} \text{ h}^{-1}$  for  $T_H$  vs.  $32.1 \pm 7.7 \text{ nmol NO}_3^- \text{ cm}^{-3} \text{ h}^{-1}$   
441 for the other ones; table 1). However, the density of denitrifiers in the sediment showed no significant differences  
442 with  $4.1 \times 10^4 \pm 1.9 \times 10^4 \text{ nosZ}$  gene copy number per ng of extracted DNA. Despite the absence of significant  
443 differences, the treatment  $T_H$  showed the highest measured microbial activity and some of the highest values of  
444 microbial abundance (supp. table 1).

445 Regarding the parameters related to MPB, the chl *a* contents were low at this period with the highest  
446 values for  $T_N$  ( $3.5 \pm 0.5 \text{ } \mu\text{g chl } a \text{ gDW}^{-1}$ ) but without any significant differences with  $T_C$ ,  $T_H$  and  $T_S$  which  
447 presented on average  $2.7 \pm 0.5 \text{ } \mu\text{g chl } a \text{ gDW}^{-1}$ . The colloidal carbohydrate EPS concentrations showed the highest  
448 values for  $T_C$  ( $36.9 \pm 10.5 \text{ } \mu\text{gEPS gDSW}^{-1}$ ) and significant lower values for the macrofauna treatments with  $13.9$   
449  $\pm 3.9 \text{ } \mu\text{g gDSW}^{-1}$  for  $T_S$  and  $18.8 \pm 9.2 \text{ } \mu\text{gEPS gDSW}^{-1}$  for  $T_H$  (table 1). The other EPS fractions showed no  
450 significant difference between treatments with on average a concentration of  $45.6 \pm 11.5 \text{ } \mu\text{g gDW}^{-1}$  for bound  
451 carbohydrate EPS, and concentrations of  $3.15 \pm 0.6$  and  $7.12 \pm 0.4 \text{ } \mu\text{g gDW}^{-1}$  respectively for the colloidal and  
452 bound fractions of protein EPS. The percentage of phaeopigments relative to total photopigments showed a  
453 significant higher value in  $T_N$  ( $54.7 \pm 5.3\%$ ) in comparison to  $T_C$  but no significant differences between control  
454 and macrofauna treatments was recorded with an average of  $49.0 \pm 7.7\%$ . Photosynthetic parameters were constant  
455 between treatment with on average a  $F_V/F_M$  of  $0.49 \pm 0.07$ , an  $\alpha$  of  $0.37 \pm 0.06$  and a  $\text{rETR}_{\text{max}}$  of  $156 \pm 49$ . The  
456 optimal irradiance ( $E_{\text{opt}}$ ) was on average of  $391 \pm 239 \text{ } \mu\text{mol photons m}^{-2} \text{ s}^{-1}$  and the saturation coefficient of light  
457 ( $E_k$ ) of  $57 \pm 17 \text{ } \mu\text{mol photons m}^{-2} \text{ s}^{-1}$ .

458

## 459 3.3. Late summer conditions

### 460 3.3.1. Sedimentary parameters

461 For each treatment ( $T_C$ ,  $T_H$ ,  $T_S$ ), the bed level analysis revealed a global net erosion of the sediment (table  
462 2; fig. 5-B). This erosion pattern was significantly stronger for  $T_S$  ( $-4.5 \pm 1.8 \text{ cm}$ ) compared to other treatments

463 and significantly weaker for  $T_H$  ( $-0.5 \pm 1.0$  cm). In the presence of *S. plana*, the silt particles appeared in lower  
 464 proportion than with other treatments (on average  $22.9 \pm 2.9\%$  for  $T_S$  vs. in mean  $30.4 \pm 4.1\%$  for  $T_H$ ,  $T_C$ , and  $T_N$ ).  
 465 The other sedimentary parameters highlighted the same significant difference for  $T_S$  which showed a higher  
 466 volumetric mass ( $1.95 \pm 0.1$  kg  $L^{-1}$ ) and dry bulk density ( $1349.4 \pm 30.3$  kg  $m^{-3}$ ), as well as a lower water content  
 467 ( $36.4 \pm 1.6\%$ ) than other treatments (table 2). The three other treatments showed on average a volumetric mass of  
 468  $1.88 \pm 0.1$  kg  $L^{-1}$ , a dry bulk density of  $1257.0 \pm 43.8$  kg  $m^{-3}$ , and a water content of  $42.0 \pm 2.8\%$ .

469 Parameters related to the SedOM showed no significant differences between treatment with on average a  
 470 TOC of  $1.49 \pm 0.43\%$ , a TN of  $0.18 \pm 0.04\%$ , and a  $\delta^{13}C$  of  $-26.34\%$ . Sediment samples contained  $63.6 \pm 3.5\%$  of  
 471 odd long chain *n*-alkanes relative to total odd *n*-alkanes and  $87.8 \pm 2.3\%$  of long chain *n*-alcohols among total *n*-  
 472 alcohols (supp. table 2).

473  
 474 **Table 2. Significant differences observed between the values measured in the control treatment ( $T_C$ ) and**  
 475 **each of the others ( $T_N$ ,  $T_H$ , and  $T_S$ ) during the late summer period.** With average and standard deviation values  
 476 as a function of *n* (given in the corresponding column). The stars given to values correspond to the significant  
 477 difference with  $T_C$  ( $p < 0.05$ : \*,  $p < 0.01$ : \*\*,  $p < 0.001$ : \*\*\*) obtained using a Tukey comparison test or a non-  
 478 parametric pairwise t-test.

Treatment	n	$T_N$	$T_C$	$T_H$	$T_S$
Bed level (cm)	48	n.d.	$-1.18 \pm 0.95$	<b><math>-0.53 \pm 1.05^*</math></b>	<b><math>-4.49 \pm 1.78^{***}</math></b>
Silt particles content (%)	9	$30.7 \pm 4.2$	$29.7 \pm 4.5$	$30.7 \pm 3.5$	<b><math>22.9 \pm 2.9^*</math></b>
Water content (%)	9	$43.2 \pm 2.5$	$41.42 \pm 3.1$	$41.4 \pm 2.6$	<b><math>36.4 \pm 1.6^*</math></b>
Dry bulk density (Csed: kg $m^{-3}$ )	9	$1237.9 \pm 39.0$	$1266.1 \pm 49.0$	$1266.8 \pm 42.8$	<b><math>1349.4 \pm 30.3^*</math></b>
Humification index (HIX)	3	$7.30 \pm 0.21$	$5.49 \pm 0.16$	$6.97 \pm 0.62$	<b><math>7.76 \pm 0.69^*</math></b>
Nitrate reduction rates (nmolNO <sub>3</sub> <sup>-</sup> cm <sup>-3</sup> h <sup>-1</sup> )	15	$100.9 \pm 13.0$	$95.4 \pm 7.3$	<b><math>77.2 \pm 9.7^*</math></b>	<b><math>72.6 \pm 8.7^{***}</math></b>

479  
 480 **3.3.2. Interstitial water parameters**  
 481 In interstitial water samples, the DOC showed low values, with on average  $4.2 \pm 1.3$  mgC  $L^{-1}$  without any  
 482 differences between treatments (supp. table 2). The BIX and FI indices showed higher values for  $T_C$  (0.8 and 1.45,  
 483 respectively) than for the other treatments (around 0.7 for BIX and 1.26 for FI). The HIX index showed a lower  
 484 value, around 6, for  $T_C$  and values around 7 for  $T_H$  and above 7 for  $T_S$  and  $T_N$ . The different nutrient concentrations  
 485 in pore water showed a high variability between replicates resulting in an absence of significance between  
 486 treatments (supp. table 2).

487  
 488 **3.3.3. Biological related parameters**  
 489 The microbial density in the sediments (bacteria and archaea) showed lower *16S rRNA* gene copy numbers  
 490 per ng of extracted DNA in  $T_S$  ( $22.7 \times 10^4 \pm 1.2 \times 10^4$ ) compared to  $T_C$ ,  $T_H$ , and  $T_N$  ( $53.2 \times 10^4 \pm 26.2 \times 10^4$ ; supp.  
 491 table 2). Archaea made up 49.8 % of the total microbial communities. This difference between treatment was also  
 492 observed for the *nosZ* genes which showed a lower abundance in  $T_S$  ( $6.0 \times 10^4 \pm 2.4 \times 10^4$ ) than in  $T_H$  and  $T_N$   
 493 ( $8.3 \times 10^4 \pm 2.8 \times 10^4$ ). In terms of microbial activity, the potential nitrate reduction rates were significantly lower



494 in presence of macrofauna ( $T_S$  and  $T_H$ ) than without ( $T_N$  and  $T_C$ ) with respectively  $74.9 \pm 9.9$  and  $98.2 \pm 10.8$   
495  $\text{nmol cm}^{-3} \text{ h}^{-1}$  (table 2). The  $\text{CO}_2$  production rate showed no differences between treatments with on average  
496  $171.0 \pm 24.2 \text{ nmol CO}_2 \text{ gDW}^{-1} \text{ h}^{-1}$ .

497 Regarding the MPB related parameters, the chlorophyll  $a$  content showed a lower content for  $T_S$  with  
498  $4.2 \pm 1.4 \mu\text{g chl } a \text{ gDSW}^{-1}$  while higher values were observed for  $T_C$ ,  $T_H$  and  $T_N$  (in mean  $6.4 \pm 0.8 \mu\text{g chl } a \text{ gDSW}^{-1}$ ;  
499 sup. table 2). The same trend was observed when analysing chl  $a$  concentration in  $\text{mg chl } a \cdot \text{m}^{-2}$ . The colloidal  
500 carbohydrate EPS concentrations showed a significant difference between  $T_S$  ( $90.9 \pm 6.6 \mu\text{gEPS gDSW}^{-1}$ ) and  $T_H$   
501 ( $77.5 \pm 3.7 \mu\text{gEPS gDSW}^{-1}$ ). The other EPS fractions showed no significant difference between treatments with  
502 on average a concentration of  $171.4 \pm 13.8 \mu\text{g gDW}^{-1}$  for bound carbohydrate EPS, and concentrations of  $2.5 \pm 0.8$   
503 and  $3.2 \pm 0.7 \mu\text{g gDW}^{-1}$  respectively for the colloidal and bound fractions of protein EPS. The percentage of  
504 phaeopigments relative to total photopigments also showed no significant differences with an average of  $68.0$   
505  $\pm 4.7\%$ . Regarding photosynthetic parameters, only the  $F_v/F_m$  showed significant lower values for  $T_S$  ( $0.42 \pm 0.13$ )  
506 while the other treatments showed a mean value of  $0.55 \pm 0.07$ . The other photosynthetic parameters were similar  
507 between treatments with a mean value of  $0.37 \pm 0.11$  and a mean  $rETR_{\text{max}}$  of  $97.1 \pm 33.5$ . The optimal irradiance  
508 ( $E_{\text{opt}}$ ) was on average of  $530.6 \pm 210 \mu\text{mol photons m}^{-2} \text{ s}^{-1}$  and the saturation coefficient of light ( $E_k$ ) of  $305.4$   
509  $\pm 118.4 \mu\text{mol photons m}^{-2} \text{ s}^{-1}$  (sup. table 2).

510

#### 511 4. Discussion

512

513 The central hypothesis of this study posited that coexisting organisms, *Hediste diversicolor* and  
514 *Scrobicularia plana*, would exert antagonistic effects on sedimentary properties, biogeochemical processes, and  
515 microbial dynamics. Our results shed light on the more intricate dynamics governing intertidal mudflats. During  
516 winter conditions, the physical parameters, especially temperature and particles deposition, exert a more significant  
517 influence, overshadowing the role played by the presence of ecosystem engineers. No significant effects were  
518 observed with the presence of *Scrobicularia plana*. However, in an unexpected way, the presence of *Hediste*  
519 *diversicolor* slightly mitigated the impacts of the physical parameters. In late summer conditions, in line with our  
520 hypothesis, our results reveal that the presence of each bioturbator strongly exert a strong influence on both biotic  
521 and abiotic parameters, with opposite effects. The presence and activity of *S. plana* led to a complete disruption of  
522 the sediment matrix, resulting in negative impacts on associated biological and especially microbial processes. In  
523 contrast, the presence and activity of *H. diversicolor* contributed to maintaining the sediment matrix and enhanced  
524 the studied biogeochemical processes. Although more in-depth measurements of bioturbation processes and the  
525 use of more precise methods will be necessary to deepen the findings on specific processes, this interdisciplinary  
526 study confirms the significant influence of ecosystem engineers in mudflats and underscores the interconnected  
527 and cumulative nature of the consequences arising from their presence on all processes simultaneously.

528

#### 529 4.1. Combined effects of temperature and presence of macrofauna in winter conditions.

530 In February, the sediment accretion in all treatments during the experiment revealed that deposition rates  
531 were stronger than erosion rates on the site. This is intricately linked to the dynamics of the estuary where currents  
532 induce erosion on the southern mudflats, and subsequently transport sediment particles towards the northern  
533 mudflats, leading predominantly to sediment accretion. This pattern being accentuated in winter by the higher

534 currents and the maximum turbidity zone located in the downstream estuary, reinforcing the amount of suspended  
535 particles (turbidity up to > 500 NTU; source: SYNAPSES network) that can settle on the upper mudflats of the  
536 estuary, especially during neap-tide periods (Le Hir et al. 2001). Thereby, it appears that the abiotic environment  
537 exerts a larger impact on the studied parameters variation than the macrofauna activities. This can be explain by  
538 the decrease of biological activities at low temperature (Georlette et al. 2004). The low temperatures that varied  
539 between -5.5 and 13.8 °C with frost events on the surface, are most likely responsible for the low measured  
540 microbial biomass, including bacteria, archaea, and MPB. For MPB, temperature is the most important factor  
541 explaining the seasonal variation of biomass and production rates (Blanchard et al. 1996). At low temperature, a  
542 decrease in the activity or deactivation of the enzymes involved in photosynthesis limits enzymatic activity by  
543 following the rules of the Arrhenius laws, consequently reducing MPB growth and primary production rates  
544 (Morgan-Kiss et al. 2006). For bacteria and archaea, frost and low temperatures on the sediment surface also play  
545 an important role in the biogeochemical process rates (Shen et al. 2020), the average microbial activity decreasing  
546 with the low temperatures, far from the optimum temperature of 15°C for production rates (Shen et al. 2015). The  
547 low temperatures also most likely resulted in a reduced activity for *S. plana* in T<sub>S</sub> regarding motility, grazing, and  
548 respiration rates, which might explain the low influence of their presence. This ecosystem engineer is known to  
549 generate an intense sediment reworking (Wiesebron et al. 2021) that was not observed through the bed level  
550 variations under the low temperature of the present study. Moreover, no active siphons were visible on the site  
551 even in the bivalve-enriched units. This is supported by previous results showing that the fauna-mediation of the  
552 sediment matrix is regulated by temperature for bivalves with an optimal value between 24 and 30 °C for *S. plana*  
553 (Hughes 1969; Brey 2001; Cozzoli et al. 2018).

554 The observed significant differences between the treatment with the addition of *H. diversicolor* and the  
555 control, especially regarding bed accretion, suggest that the influence of this species on the surrounding  
556 environment was not inhibited by environmental factors. This resulted in cumulative effects of both winter  
557 conditions and bio-irrigation by this gallery-diffuser on the measured parameters. *H. diversicolor* can tolerate wide  
558 temperature fluctuations (Wolff 1973) with reduced food-searching activity only occurring below 8°C (Scaps  
559 2002). Furthermore, its bioirrigation rates are not temperature-dependent (Sanz-Lázaro et al. 2011). This species  
560 inhabits burrows lined with mucus-filled galleries that extend over 10 cm into the sediment (Davey 1994).  
561 Temperature fluctuations at this depth tend to be more moderate, consistent with our observed temperature profiles,  
562 and explaining their tolerance to low environmental temperature. Therefore, it can be asserted that temperature  
563 during the winter manipulative experiment doesn't significantly decrease the activity of *H. diversicolor*, especially  
564 considering the insulating effect of their mucus secretions, known to confer resistance to cold conditions (Hawes  
565 et al. 2010). In addition to constructing mucus-lined galleries, *H. diversicolor* releases mucus during its feeding  
566 activities by using a mucous trapping-net even at a temperature of 5°C (Riisgård et al. 1992). This mucus secretion  
567 were shown to trap particles as much as during high tide where they behave as filter-feeders and at low tide where  
568 they switch to deposit-feeding (Esselink and Zwarts 1989; Esnault et al. 1990; Riisgard 1991a; Scaps 2002). These  
569 mucus secretions, functioning as sediment traps, most likely explain the significantly higher sediment  
570 accumulation observed in the T<sub>H</sub> treatment. However, the mucus released by *H. diversicolor* at the sediment  
571 surface was not detected in our study, as no significant differences in EPS concentrations were observed between  
572 T<sub>H</sub> and T<sub>C</sub> (supp. table 1). Nonetheless, this multidisciplinary study revealed a notable impact of *H. diversicolor*  
573 on the microbial community. T<sub>H</sub> treatments exhibited higher values for microbial-related parameters compared to

574 T<sub>C</sub> and T<sub>S</sub> (supp. table 1), indicating enhanced microbial growth and activity. The preference of microbes for EPS  
575 as a carbon source (Bouillon and Boschker 2006; Bellinger et al. 2009; Taylor et al. 2013; Morelle et al. 2022)  
576 likely led to rapid EPS consumption in the presence of *H. diversicolor*, resulting in non-detectable EPS levels.  
577 This assumption is further supported by the slightly higher average DOC values in T<sub>H</sub> treatment compared to T<sub>C</sub>  
578 (+7.7%) and T<sub>S</sub> (+28.8%; supp. table 1), suggesting a higher degradation of labile OM (Perkins et al. 2022).  
579 Although not statistically significant, this aligns with slightly higher average NH<sub>4</sub><sup>+</sup> concentrations in pore water  
580 samples from T<sub>H</sub> compared to T<sub>C</sub> (+9%) and T<sub>S</sub> (+5.6%; supp. table 1). Microbes involved in nitrate reduction  
581 appeared to benefit from the presence of *H. diversicolor*, as evidenced by the significantly higher nitrate reduction  
582 rates and, although not reaching statistical significance (p = 0.13), the slightly higher abundance of *nosZ* genes in  
583 T<sub>H</sub>, respectively 48% and 42% higher than in T<sub>S</sub> and T<sub>C</sub> (supp. Table 1). This also aligns with the lower, though  
584 not statistically significant (p = 0.7), average in NO<sub>3</sub><sup>-</sup> concentrations measured in the pore water samples from T<sub>H</sub>  
585 with an average 15% lower than T<sub>C</sub> (supp. table 1). This difference between T<sub>H</sub> and the other treatments may be  
586 attributed to bioirrigation activities. As demonstrated in various sediment dwellers (e.g., bivalves, worms,  
587 crustaceans, echinids), bioturbation directly stimulates nutrient release at the sediment-water interface (Eriksson  
588 et al. 2017). Nematodes have also been shown to enhance bacterial activity and nutrient fluxes by frequently  
589 ventilating galleries across the sediment-water interface (D'Hondt et al. 2018). In our case, the bioirrigation  
590 performed by *H. diversicolor* (Kristensen and Hansen 1999) is known to enhance oxygen penetration, thereby  
591 promoting aerobic and anaerobic organic matter remineralization, which likely stimulated bacterial productivity  
592 and nutrient release (Richard et al. 2023). Even in winter conditions, when ventilation rates of *H. diversicolor* may  
593 decrease (Kristensen 1983; Riisgård et al. 1992; Vedel 1998), our results showed that their presence still exerts an  
594 influence on the surrounding environment.

595 Significantly higher values of EPS concentrations were observed in the control treatment (T<sub>C</sub>) in  
596 concomitance with lower values of the humification index HIX and higher values of the fluorescence indices BIX  
597 and FI (table 1). The reworking, reshaping, and flattening of the sediments may have disturbed the sediment matrix  
598 and MPB biofilm. This hypothesis is confirmed by the significantly lower values of chl *a* measured in T<sub>C</sub>, T<sub>H</sub>, and  
599 T<sub>S</sub>, in comparison to T<sub>N</sub> (Table 1). In those conditions, MPB cells would have to build new pioneering biofilms by  
600 performing migration, this process occurring during a lag phase of several days (Yallop et al. 2000; Orvain et al.  
601 2014). In T<sub>C</sub>, the high values of carbohydrate EPS must have played a role in the migrating movement of epipellic  
602 benthic diatoms and contributed to the adhesion of microalgae at the sediment surfaces by forming biofilms. This  
603 was supported by the values of the fluorescence indices, suggesting the presence of a more freshly and microbially  
604 produced less aromatic DOM (McKnight et al. 2001) which could be attributed to a higher EPS production by  
605 MPB. This assumption was support by Li et al. (2023) showing that microbial EPS showed higher BIX and FI  
606 concomitant with lower HIX than more aromatic products with values in the range of our results. The absence of  
607 such trends in the treatments with macrofaunal addition (T<sub>S</sub> and T<sub>H</sub>) could be attributed to the feeding activity of  
608 the ecosystem engineers which, despite an apparent reduced activity for *S. plana*, must continue to feed on the OM  
609 pool.

610

#### 611 4.2. Intense top-down impact of macrofauna in late summer conditions

612 In late summer, the addition of *S. plana* individuals led to a coarser sediment structure (table 2),  
613 suggesting that the reworking activity of the bivalves led to the bioresuspension of fine sediment particles. This is

614 confirmed by the temporal changes of the bed topography, which showed a significant loss by erosion in this  
615 treatment (fig. 5). In addition to particle size, the sediment reworking performed by *S. plana* also significantly  
616 affected most of the sedimentary parameters (volumetric mass, dry bulk density, and water content; table 2). These  
617 results highlight the considerable effects of the *S. plana* activities on the sedimentary matrix at this season. This is  
618 in line with the literature showing that the biological activity for bivalves and the related impacts on the  
619 sedimentary matrix are important and dependent on temperature (Brown et al. 2004; Cozzoli et al. 2020, 2021;  
620 Wiesebron et al. 2021). The modelled sediment loss resulting from *S. plana* activities was estimated at 50 cm year<sup>-1</sup>  
621 in the Marennes-Oléron Bay (Orvain et al. 2012). Considering the seasonal changes and the optima of this species  
622 for temperature, our results were in accordance with this estimation, showing an impact of *S. plana* on the  
623 sedimentary matrix corresponding to a sediment loss of 3 cm in 1 week. These effects were likely mainly due to  
624 the biological activities of *S. plana* related to burrowing and/or nutrition activities, which consist in siphoning the  
625 sediment surface that surrounds its semi-permanent burrow (Orvain 2005), continuously consuming the MPB  
626 during the low tide (Hughes 1969). The low chl *a* content measured in T<sub>S</sub> could thereby most likely be due to an  
627 elevated foraging activity. However, in our study, the phaeopigment percentages, which represent the degraded  
628 compounds of chl *a*, were not different in T<sub>S</sub> compared to other treatments (supp. table 2). Such a difference would  
629 have been expected as the result of a more intense predation pressure. The absence of effects on phaeopigments  
630 might be due to the rapid diffusion and/or resuspension of these pigments due to a high hydrodynamic stress as  
631 already suggested by Anand et al. (2014). This could also include resuspension of benthic diatoms, which in this  
632 case would apply to all treatments. In addition, the low chl *a* content could be an indirect effect of *S. plana* due to  
633 the strong disruption of the sediment matrix, which might limit the formation of structured MPB biofilms and in  
634 turn reduce photosynthesis and biomass production (Morelle et al. 2020). This assumption is supported by the  
635 lower values of the maximum effective quantum yield of the PSII ( $F_v/F_M$ ) measured in T<sub>S</sub> than in other treatments.  
636 Indeed, this result suggests that MPB was not in optimal conditions for photosynthesis since this rate depends on  
637 the physiological status of the biofilm (Serôdio et al. 2007). Such indirect negative impact of *S. plana* on the  
638 biological compartment was also observed in the microbial abundances and activity. Indeed, the T<sub>S</sub> showed low  
639 microbial abundance both for bacteria and archaea (*16S rRNA* copy numbers) and the lowest activity in terms of  
640 nitrate reduction rates. This suggests that the presence of *S. plana* at such density (440 ind m<sup>-2</sup>) in summer resulted  
641 in an intense sediment reworking almost completely inhibiting the biological components at the basis of the benthic  
642 trophic network of the intertidal mudflats. However, the present densities tested were the highest found for this  
643 species in the studied mudflat, and the activity of *S. plana* was somewhat slowed down by temperature (as seen in  
644 our winter results). Thereby, it's likely that this destructive impact is usually less pronounced compared to what  
645 we observed during our late-summer experiment. In addition, this effect must also be lower by the intense predation  
646 pressure that this bivalve receives from the upper compartment of the trophic network which can result in a strong  
647 reduction of siphon extension and feeding activity for bivalves (Maire et al. 2010).

648 In contrast, the treatment with *H. diversicolor* showed the lowest bed level erosion (fig. 5), thereby  
649 suggesting that the presence of polychaetes limit particle resuspension due to biostabilisation effects by mucus  
650 secretion which can result in a relative bed accretion (Riisgard 1991b; Passarelli et al. 2012). In this survey, since  
651 the sediment parameters were not significantly different compared to T<sub>N</sub> and T<sub>C</sub>, we suggest that the activity of *H.*  
652 *diversicolor* improved the stability of the sediments and, thus, attenuated the erosion, rather than promoting  
653 sediment accumulation. The fact that the presence of *H. diversicolor* reduced sediment erosion rates must also

654 have limited the MPB biofilm resuspension (Andersen et al. 2010; Donadi et al. 2013) and played a role in the  
655 high level of MPB biomass that was observed (table 2). Despite the predation pressure exerted by *H. diversicolor*  
656 (Scaps 2002), the chl *a* concentrations were similar to the natural and control treatments (T<sub>N</sub> and T<sub>C</sub>). This could  
657 be explained by a balance existing between the decrease in MPB biomass related to the feeding activity of  
658 *H. diversicolor* and the increase in the biomass related to their bioirrigation activities (Asmus and Bauerfeind 1994;  
659 Fernandes et al. 2006; Morelle et al. 2021; Richard et al. 2023). In the present case, enhancement of nutrients  
660 fluxes through bioirrigation of *H. diversicolor* (Kristensen and Hansen 1999) may have promoted bacterial  
661 productivity and MPB growth, which in turn may have decreased the vulnerability to erosion and promoted  
662 sediment accumulation through additional EPS production (Widdows et al. 2004; Andersen et al. 2010). Indeed, a  
663 higher abundance of both *16S rRNA* genes (bacteria, archaea) and *nosZ* genes (denitrifiers) was observed in the  
664 T<sub>H</sub> treatments compared to T<sub>C</sub> and T<sub>N</sub>, suggesting a stimulation process of microbial growth by *H. diversicolor*.  
665 This might be due to a higher degradation rate of OM in the presence of *H. diversicolor* related to the higher  
666 oxygen penetration with bioirrigation activities (Pischedda et al. 2012). However, this potential increase in  
667 degradation activity was not observed in the microbial activity measured at the end of the experiment (CO<sub>2</sub>  
668 production and nitrate reduction rates) which showed higher values in T<sub>C</sub>. Moreover, higher values of HIX as well  
669 as lower values of BIX and FI in T<sub>H</sub> than in T<sub>C</sub> suggest an increase in DOM aromaticity related to the presence of  
670 *H. diversicolor* and/or to the use, consumption, or transformation of components of lower aromaticity (Aller 1980;  
671 Zhang et al. 2022). Indeed, such an increase could be explained by the transfer of more degraded organic material  
672 from deeper sediment to the surface (also significant and pertinent for the T<sub>S</sub> treatment). This is in line with the  
673 observations made by He et al. (2019), who showed that bioturbation activities accelerated the DOM release,  
674 mainly composed of aromatic/mature material (higher HIX), from sediment to overlying water with bioturbation.  
675 He et al. (2019) also reported changes in DOM composition over time, with an increase of microbially-produced  
676 DOM resulting from bacterial growth and propagation by bioturbation. In the present study, microbial production  
677 of DOM was not observed through the fluorescence indices, as the FI values corroborate a more terrestrial/mature  
678 character of DOM in the enriched treatments, in line with the HIX variations (table 2). Overall, the HIX and FI  
679 values were low and BIX values high, reflecting a mixture of organic material of low aromaticity and moderate to  
680 strong autochthonous sources with more mature and hydrophobic DOM components (Huguet et al. 2009). These  
681 results are consistent with those reported by Bowen et al. (2017) in the pore waters of California intertidal wetlands  
682 and by Burdige et al. (2004) in marine surface sediments, with autochthonous aquatic DOM predominant in surface  
683 waters and more terrestrial/refractory material in deeper pore waters. Nevertheless, the nature of sedimentary OM  
684 remains the same whatever the season and the treatment, with a strong terrestrial imprint. This is shown by both  
685 bulk and molecular analyses, with depleted δ<sup>13</sup>C values of sedimentary OM and the predominance of long-chain  
686 *n*-alkanes and *n*-alcohols derived from terrestrial plants vs. short-chain homologues (Bianchi and Canuel 2011).  
687 Such results converge with the general view that terrestrial OM is refractory and well-preserved in sediments, in  
688 contrast with OM components produced *in situ*, considered as labile and less abundant in sediments (e.g., Burdige  
689 2007). Nevertheless, the lower BIX values in T<sub>H</sub> than in T<sub>C</sub> suggested that the freshly produced DOM was  
690 used/consumed, degraded, or released in surficial water. Thereby, we assumed that, during the experiment, the  
691 presence of *H. diversicolor* stimulated the degradation of low aromatic compounds, as the latter are, by nature,  
692 more rapidly and easily degraded (Hansen et al. 2016). This is in line with the increase in microbial abundance  
693 and the decrease in DOM aromaticity (lower HIX) observed in T<sub>H</sub>. The rapid depletion of easily degradable

694 compounds in pore waters, and the release of such compounds in surficial water favoured by bioirrigation of *H.*  
695 *diversicolor*, thus explain that the microbial production of DOM was not observed through the fluorescence  
696 analyses. Thereby, our results suggested that the activity of *H. diversicolor* had positive effects on both the  
697 sedimentary matrix and on microbial carbon fluxes, despite its high density and consequent predatory activity.

698

## 699 **5. Conclusions**

700 The influence of two intertidal bioturbators, *H. diversicolor* and *S. plana*, on the sedimentary,  
701 biogeochemical, and microbial dynamics was evaluated through field manipulative experiments during the two  
702 most contrasted seasons in a temperate estuarine mudflat. The present study confirmed the importance of  
703 temperature and water flow regimes both on macrofauna activity and microbial dynamics in intertidal mudflat. In  
704 the two different situations (either high sediment deposition and low temperature in winter, or high erosion and  
705 temperature under late summer conditions), the presence or absence of the bioturbators was shown to modify the  
706 sediment particle grain size composition and bed topography, with the erosion/accretion of the sediment partly  
707 related to the nutrition and burrowing activities of the species. The bioturbators were also observed to have a  
708 simultaneous influence on most of the studied parameters in the surficial sediment layer – with a direct or indirect  
709 impact on the pore water DOM quality, the growth, and activities of microorganisms (i.e., bacteria, archaea, and  
710 MPB). This study showed that some links between the different compartments are difficult to highlight without  
711 studying all components reinforcing the interest of conducting interdisciplinary studies to consider a maximum of  
712 biological and physicochemical variables to improve the understanding of ecosystem functioning. This study also  
713 highlights the importance of biological control of sedimentary systems on tidal flats, even in macrotidal estuaries.  
714 This is critical to improve management and conservation policies of estuarine ecosystems by better integrating the  
715 functional roles and bioturbation of dominating macrofauna, to restore the productivity of the intertidal zones, and  
716 to develop new models coupling biogeochemistry and benthic processes to sediment dynamics able to produce  
717 more realistic scenarios in the context of the global warming.

718

## 719 **Acknowledgments:**

720 This study was funded by the PHARESEE<sup>©</sup> project (Program GIP Seine-Aval 6) which aims to better  
721 understand, for modelling and restoration purposes, the links existing between hydrosedimentary, biogeochemical  
722 and microbial dynamics on mudflats ecosystems. The authors want to thank the GIP Seine-Aval agency, especially  
723 N. Bacq. Thank you to Jean Paul Lehodey (CREC) & Jean-Marc Paint (IUT Grand Ouest Normandie) for their  
724 help in the field systems conception and to the people who actively participated in sampling and/or analyses,  
725 especially Thomas Lecarpentier (Maison de l'Estuaire), Mathieu Chauveau, Guillaume Izabel, Guillaume Bouger,  
726 Amelie Gaigaerd, Cedric Fouillet, Véronique Vaury, Johanne Lebrun-Thauront, Kéline Judith, Jessica Maubert,  
727 Sarah Adeline, Théo Chiron, Camille Duchemin, Enora Logodin, Clémence Paucis, Amaury Tuon, Michel Simon  
728 and Romain Levailant. We are also thankful to Virginie Daburon who performed genetic analyses of microbial  
729 DNA from sediment at the molecular ecology platform (UMR 6553 Ecobio, Rennes, CNRS/UR1), Marion Chorin  
730 for the nutrient analyses at the EcoChimie Platform (EcoChim) from UMS OSUR 3343, and David Moussa,  
731 chemical engineer at Rouen University (M2C-Rouen) for providing nutrients and TOC chemical analysis. Authors  
732 thank the support of CESAM (UIDP/50017/2020 + UIDB/50017/2020 + LA/P/0094/2020).

733

734 **References**

- 735 Admiraal, W., and H. Peletier. 1980. Influence of Seasonal Variations of Temperature and Light on the Growth  
736 Rate of Cultures and Natural Populations of Intertidal Diatoms \*. **2**: 35–43.
- 737 Aller, R. C. 1980. Diagenetic Processes Near the Sediment-Water Interface of Long Island Sound. I.:  
738 Decomposition and Nutrient Element Geochemistry (S, N, P), p. 237–350. *In* B.B.T.-A. in G. Saltzman [ed.],  
739 Estuarine Physics and Chemistry: Studies in Long Island Sound. Elsevier.
- 740 Aller, R. C. 1988. Benthic fauna and biogeochemical processes in marine sediments: The role of burrow structures.  
741 Nitrogen Cycl. Coast. Mar. Environ. 301–341.
- 742 Aller, R. C., and J. K. Cochran. 2019. The critical role of bioturbation for particle dynamics, priming potential,  
743 and organic c remineralization in marine sediments: Local and basin scales. *Front. Earth Sci.* **7**: 1–14.  
744 doi:10.3389/feart.2019.00157
- 745 Anand, S. S., K. J. Anju, D. Mathew, and M. D. Kumar. 2014. Sub-hourly changes in biogeochemical properties  
746 in surface waters of Zuari estuary, Goa. *Environ. Monit. Assess.* **186**: 719–724. doi:10.1007/s10661-013-  
747 3410-1
- 748 Andersen, T. J., M. Lanuru, C. Van Bernem, M. Pejrup, and R. Riethmueller. 2010. Erodibility of a mixed mudflat  
749 dominated by microphytobenthos and *Cerastoderma edule*, East Frisian Wadden Sea, Germany. *Estuar.*  
750 *Coast. Shelf Sci.* **87**: 197–206. doi:10.1016/j.ecss.2009.10.014
- 751 Asmus, R. M., and E. Bauerfeind. 1994. The microphytobenthos of Königshafen - spatial and seasonal distribution  
752 on a sandy tidal flat. *Helgolander Meeresuntersuchungen* **48**: 257–276.
- 753 Behrenfeld, M. J., O. Prasil, M. Babin, and F. Bruyant. 2004. in Search of a Physiological Basis for Covariations  
754 in Light-Limited and Light-Saturated Photosynthesis1. *J. Phycol.* **40**: 4–25. doi:10.1046/j.1529-  
755 8817.2004.03083.x
- 756 Bellinger, B. J., G. J. C. Underwood, S. E. Ziegler, and M. R. Gretz. 2009. Significance of diatom-derived polymers  
757 in carbon flow dynamics within estuarine biofilms determined through isotopic enrichment. *Aquat. Microb.*  
758 *Ecol.* **55**: 169–187. doi:10.3354/ame01287
- 759 Bianchi, T. S., and E. A. Canuel. 2011. Chemical biomarkers in aquatic ecosystems, Princeton University Press.
- 760 Blanchard, G. F., J.-M. Guarini, P. Richard, P. Gros, and F. Mornet. 1996. Quantifying the short-term temperature  
761 effect on light-saturated photosynthesis of intertidal microphytobenthos. *Mar Ecol Prog Ser* **134**: 309–313.  
762 doi:10.3354/meps134309
- 763 Boudreau, B. P., and B. B. Jorgensen. 2001. The benthic boundary layer: Transport processes and biogeochemistry,  
764 Oxford Uni. Oxford University Press.
- 765 Bouillon, S., and H. T. S. Boschker. 2006. Bacterial carbon sources in coastal sediments: a review based on stable  
766 isotope data of biomarkers. *Biogeosciences* **3**: 175–185. doi:10.5194/bgd-2-1617-2005
- 767 Bowen, J. C., C. D. Clark, J. K. Keller, and W. J. De Bruyn. 2017. Optical properties of chromophoric dissolved  
768 organic matter (CDOM) in surface and pore waters adjacent to an oil well in a southern California salt marsh.  
769 *Mar. Pollut. Bull.* **114**: 157–168. doi:10.1016/j.marpolbul.2016.08.071
- 770 Bradford, M. M. 1976. A rapid and sensitive method for the quantitation of microgram quantities of protein  
771 utilizing the principle of protein-dye binding. *Anal. Biochem.* **72**: 248–254.
- 772 Brey, T. 2001. Population dynamics in benthic invertebrates. A virtual handbook. [http://www. awi-bremerhaven.](http://www.awi-bremerhaven.de/Benthic/Ecosystem/FoodWeb/Handbook/main.html)  
773 [de/Benthic/Ecosystem/FoodWeb/Handbook/main. html.](http://www.awi-bremerhaven.de/Benthic/Ecosystem/FoodWeb/Handbook/main.html) Alfred Wegener Inst. Polar Mar. Res. Ger.

774 Brown, J. H., J. F. Gillooly, A. P. Allen, V. M. Savage, and G. B. West. 2004. Response to Forum Commentary  
775 on " Toward a Metabolic Theory of Ecology ". *Ecology* **85**: 1818–1821.

776 Bruno, J. F., and M. Bertness. 2001. Habitat modification and facilitation in benthic marine communities. *Mar.*  
777 *community Ecol.*

778 Burdige, D. J. 2007. Preservation of organic matter in marine sediments: Controls, mechanisms, and an imbalance  
779 in sediment organic carbon budgets? *Chem. Rev.* **107**: 467–485. doi:10.1021/cr050347q

780 Burdige, D. J., S. W. Kline, and W. Chen. 2004. Fluorescent dissolved organic matter in marine sediment pore  
781 waters. *Mar. Chem.* **89**: 289–311. doi:10.1016/j.marchem.2004.02.015

782 Burdige, D. J., and T. Komada. 2015. Sediment Pore Waters, p. 535–577. *In* D.A. Hansell and C.A. Carlson [eds.],  
783 *Biogeochemistry of marine dissolved organic matter*. Burlington: Academic Press.

784 Cartaxana, P., M. Ruivo, C. Hubas, I. Davidson, J. Serôdio, and B. Jesus. 2011. Physiological versus behavioral  
785 photoprotection in intertidal epipellic and epipsammic benthic diatom communities. *J. Exp. Mar. Bio. Ecol.*  
786 **405**: 120–127. doi:10.1016/j.jembe.2011.05.027

787 Chennu, A., P. Färber, G. De'ath, D. De Beer, and K. E. Fabricius. 2017. A diver-operated hyperspectral imaging  
788 and topographic surveying system for automated mapping of benthic habitats. *Sci. Rep.* **7**: 1–12.  
789 doi:10.1038/s41598-017-07337-y

790 Chennu, A., N. Volkenborn, D. De Beer, D. S. Wetthey, S. A. Woodin, and L. Polerecky. 2015. Effects of  
791 bioadvection by *Arenicola marina* on microphytobenthos in permeable sediments. *PLoS One* **10**: 1–16.  
792 doi:10.1371/journal.pone.0134236

793 Claquin, P., I. Probert, S. Lefebvre, and B. Veron. 2008. Effects of temperature on photosynthetic parameters and  
794 TEP production in eight species of marine microalgae. *Aquat. Microb. Ecol.* **51**: 1–11.  
795 doi:10.3354/ame01187

796 Coffinet, S., A. Huguet, C. Anquetil, and others. 2017. Evaluation of branched GDGTs and leaf wax n-alkane  $\delta^{2}H$   
797 as (paleo) environmental proxies in East Africa. *Geochim. Cosmochim. Acta* **198**: 182–193.  
798 doi:10.1016/j.gca.2016.11.020

799 Van Colen, C., F. Montserrat, M. Vincx, P. M. J. Herman, T. Ysebaert, and S. Degraer. 2010. Macrobenthos  
800 recruitment success in a tidal flat: Feeding trait dependent effects of disturbance history. *J. Exp. Mar. Bio.*  
801 *Ecol.* **385**: 79–84. doi:10.1016/j.jembe.2010.01.009

802 Colijn, F., and K. S. Dijkema. 1981. Species Composition of Benthic Diatoms and Distribution of Chlorophyll a  
803 on an Intertidal Flat in the Dutch Wadden Sea. *Mar. Ecol. Prog. Ser.* **4**: 9–21.

804 Cozzoli, F., T. J. Bouma, P. Ottolander, M. S. Lluch, T. Ysebaert, and P. M. J. Herman. 2018. The combined  
805 influence of body size and density on cohesive sediment resuspension by bioturbators. *Sci. Rep.* **8**: 1–12.  
806 doi:10.1038/s41598-018-22190-3

807 Cozzoli, F., T. Gomes da Conceição, J. Van Dalen, and others. 2020. Biological and physical drivers of bio-  
808 mediated sediment resuspension: A flume study on *Cerastoderma edule*. *Estuar. Coast. Shelf Sci.* **241**.  
809 doi:10.1016/j.ecss.2020.106824

810 Cozzoli, F., M. Shokri, T. Gomes da Conceição, and others. 2021. Modelling spatial and temporal patterns in  
811 bioturbator effects on sediment resuspension: A biophysical metabolic approach. *Sci. Total Environ.* **792**:  
812 148215. doi:10.1016/j.scitotenv.2021.148215

813 Crain, C. M., and M. D. Bertness. 2006. *Ecosystem Engineering across Environmental Gradients : Implications*



814 for Conservation and Management. *Bioscience* **56**: 211–218.

815 D’Hondt, A. S., W. Stock, L. Blommaert, T. Moens, and K. Sabbe. 2018. Nematodes stimulate biomass  
816 accumulation in a multispecies diatom biofilm. *Mar. Environ. Res.* **140**: 78–89.  
817 doi:10.1016/j.marenvres.2018.06.005

818 Dauwe, B., P. M. J. Herman, and C. H. R. Heip. 1998. Community structure and bioturbation potential of  
819 macrofauna at four North Sea stations with contrasting food supply. *Mar. Ecol. Prog. Ser.* **173**: 67–83.  
820 doi:10.3354/meps173067

821 Davey, J. T. 1994. The architecture of the burrow of *Nereis diversicolor* and its quantification in relation to  
822 sediment-water exchange. *J. Exp. Mar. Bio. Ecol.* **179**: 115–129. doi:10.1016/0022-0981(94)90020-5

823 Davison, I. R. 1991. Environmental Effects on Algal Photosynthesis: Temperature. *J. Phycol.* **27**: 2–8.  
824 doi:10.1111/1529-8817.ep10868724

825 Derrien, M., K. H. Shin, and J. Hur. 2019. Biodegradation-induced signatures in sediment pore water dissolved  
826 organic matter: Implications from artificial sediments composed of two contrasting sources. *Sci. Total*  
827 *Environ.* **694**: 133714. doi:10.1016/j.scitotenv.2019.133714

828 Donadi, S., J. Westra, E. J. Weerman, and others. 2013. Non-trophic Interactions Control Benthic Producers on  
829 Intertidal Flats. *Ecosystems* **16**: 1325–1335. doi:10.1007/s10021-013-9686-8

830 Dubois, M., K. A. Gilles, J. K. Hamilton, Pa. Rebers, and F. Smith. 1956. Colorimetric method for determination  
831 of sugars and related substances. *Anal. Chem.* **28**: 350–356.

832 Eglinton, G., and R. J. Hamilton. 1967. Leaf epicuticular waxes. *Science* (80-. ). **156**: 1322–1335.

833 Einfeldt, A. L., J. R. Doucet, and J. A. Addison. 2014. Phylogeography and cryptic introduction of the ragworm  
834 *Hediste diversicolor* (Annelida, Nereididae) in the Northwest Atlantic. *Invertebr. Biol.* **133**: 232–241.  
835 doi:10.1111/ivb.12060

836 Eriksson, B. K., J. Westra, I. Van Gerwen, and others. 2017. Facilitation by ecosystem engineers enhances nutrient  
837 effects in an intertidal system. *Ecosphere* **8**. doi:10.1002/ecs2.2051

838 Esnault, G., C. Retiere, and R. Lambert. 1990. Food resource partitioning in a population of *Nereis diversicolor*  
839 (Annelida, Polychaeta) under experimental conditions. *Trophic Relationships Mar. Environ.* **453467**: 453–  
840 467.

841 Esselink, P., and L. Zwarts. 1989. Seasonal trend in burrow depth and tidal variation in feeding activity of *Nereis*  
842 *diversicolor*. *Mar. Ecol. Prog. Ser.* **56**: 243–254.

843 Fanjul, E., M. Escapa, D. Montemayor, M. Addino, M. F. Alvarez, M. A. Grela, and O. Iribarne. 2015. Effect of  
844 crab bioturbation on organic matter processing in South West Atlantic intertidal sediments. *J. Sea Res.* **95**:  
845 206–216. doi:10.1016/j.seares.2014.05.005

846 Fernandes, S., P. Sobral, and M. H. Costa. 2006. *Nereis diversicolor* effect on the stability of cohesive intertidal  
847 sediments. *Aquat. Ecol.* **40**: 567–579. doi:10.1007/s10452-005-8000-z

848 François, F., M. Gerino, G. Stora, J. P. Durbec, and J. C. Poggiale. 2002. Functional approach to sediment  
849 reworking by gallery-forming macrobenthic organisms: Modeling and application with the polychaete  
850 *Nereis diversicolor*. *Mar. Ecol. Prog. Ser.* **229**: 127–136. doi:10.3354/meps229127

851 Georgette, D., V. Blaise, T. Collins, and others. 2004. Some like it cold: Biocatalysis at low temperatures. *FEMS*  
852 *Microbiol. Rev.* **28**: 25–42. doi:10.1016/j.femsre.2003.07.003

853 Hansen, A. M., T. E. C. Kraus, B. A. Pellerin, J. A. Fleck, B. D. Downing, and B. A. Bergamaschi. 2016. Optical

854 properties of dissolved organic matter (DOM): Effects of biological and photolytic degradation. *Limnol.*  
855 *Oceanogr.* **61**: 1015–1032. doi:10.1002/lno.10270

856 Hawes, T. C., M. R. Worland, and J. S. Bale. 2010. Freezing in the Antarctic limpet, *Nacella concinna*.  
857 *Cryobiology* **61**: 128–132. doi:10.1016/j.cryobiol.2010.06.006

858 He, Y., B. Men, X. Yang, Y. Li, H. Xu, and D. Wang. 2019. Relationship between heavy metals and dissolved  
859 organic matter released from sediment by bioturbation/bioirrigation. *J. Environ. Sci. (China)* **75**: 216–223.  
860 doi:10.1016/j.jes.2018.03.031

861 Hellequin, E., C. Monard, A. Quaiser, M. Henriot, O. Klarzynski, and F. Binet. 2018. Specific recruitment of soil  
862 bacteria and fungi decomposers following a biostimulant application increased crop residues mineralization.  
863 *PLoS One* **13**: 1–19. doi:10.1371/journal.pone.0209089

864 Le Hir, P., A. Ficht, R. S. Jacinto, and others. 2001. Fine Sediment Transport and Accumulations at the Mouth of  
865 the Seine Estuary (France). *Estuaries* **24**: 950. doi:10.2307/1353009

866 Hope, J. A., D. M. Paterson, and S. F. Thrush. 2020. The role of microphytobenthos in soft-sediment ecological  
867 networks and their contribution to the delivery of multiple ecosystem services. *J. Ecol.* **108**: 815–830.  
868 doi:10.1111/1365-2745.13322

869 Hughes, R. N. 1969. A study of feeding in *Scrobicularia plana*. *J. Mar. Biol. Assoc. United Kingdom* **49**: 805–823.

870 Huguet, A., L. Vacher, S. Relexans, S. Saubusse, J. M. Froidefond, and E. Parlanti. 2009. Properties of fluorescent  
871 dissolved organic matter in the Gironde Estuary. *Org. Geochem.* **40**: 706–719.  
872 doi:10.1016/j.orggeochem.2009.03.002

873 Jones, C. G., J. H. Lawton, and M. Shachak. 1994. Organisms as ecosystem engineers. *OIKOS* **69**: 373–386.

874 Jones, C. M., D. R. H. Graf, D. Bru, L. Philippot, and S. Hallin. 2013. The unaccounted yet abundant nitrous oxide-  
875 reducing microbial community: A potential nitrous oxide sink. *ISME J.* **7**: 417–426.  
876 doi:10.1038/ismej.2012.125

877 Juneau, P., A. Barnett, V. Méléder, C. Dupuy, and J. Lavaud. 2015. Combined effect of high light and high salinity  
878 on the regulation of photosynthesis in three diatom species belonging to the main growth forms of intertidal  
879 flat inhabiting microphytobenthos. *J. Exp. Mar. Bio. Ecol.* **463**: 95–104. doi:10.1016/j.jembe.2014.11.003

880 Van De Koppel, J., T. Van Der Heide, A. H. Altieri, B. K. Eriksson, T. J. Bouma, H. Olf, and B. R. Silliman.  
881 2015. Long-Distance Interactions Regulate the Structure and Resilience of Coastal Ecosystems. *Ann. Rev.*  
882 *Mar. Sci.* **7**: 139–158. doi:10.1146/annurev-marine-010814-015805

883 Kristensen, E. 1983. Ventilation and oxygen uptake by three species of. *Mar. Ecol. Prog. Ser.* **12**: 299–305.

884 Kristensen, E., G. Penha-lobes, M. Delefosse, T. Valdemarsen, C. O. Quintana, and G. T. Banta. 2012. What is  
885 bioturbation? The need for a precise definition for fauna in aquatic sciences. **446**: 285–302.  
886 doi:10.3354/meps09506

887 Kristensen, K., and K. Hansen. 1999. Transport of carbon dioxide and ammonium in bioturbated (*Nereis*  
888 *diversicolor*) coastal, marine sediments. *Biogeochemistry* **45**: 147–168.

889 Laverman, A. M., P. Van Cappellen, D. Van Rotterdam-Los, C. Pallud, and J. Abell. 2006. Potential rates and  
890 pathways of microbial nitrate reduction in coastal sediments. *FEMS Microbiol. Ecol.* **58**: 179–192.  
891 doi:10.1111/j.1574-6941.2006.00155.x

892 Laverman, A. M., C. Pallud, J. Abell, and P. Van Cappellen. 2012. Comparative survey of potential nitrate and  
893 sulfate reduction rates in aquatic sediments. *Geochim. Cosmochim. Acta* **77**: 474–488.

894 doi:10.1016/j.gca.2011.10.033

895 Li, W., X. Li, C. Han, L. Gao, H. Wu, and M. Li. 2023. A new view into three-dimensional excitation-emission  
896 matrix fluorescence spectroscopy for dissolved organic matter. *Sci. Total Environ.* **855**: 158963.  
897 doi:10.1016/j.scitotenv.2022.158963

898 Lorenzen, C. J. 1967. Determination of Chlorophyll and Pheo-Pigments : Spectrophotometric Equations. *Limnol.*  
899 *Oceanogr.* **12**: 343–346. doi:10.4319/lo.1967.12.2.0343

900 Maire, O., J. N. Merchant, M. Bulling, L. R. Teal, A. Grémare, J. C. Duchêne, and M. Solan. 2010. Indirect effects  
901 of non-lethal predation on bivalve activity and sediment reworking. *J. Exp. Mar. Bio. Ecol.* **395**: 30–36.  
902 doi:10.1016/j.jembe.2010.08.004

903 Marchesi, J. R., T. Sato, A. J. Weightman, T. A. Martin, J. C. Fry, S. J. Hiom, and W. G. Wade. 1998. Design and  
904 evaluation of useful bacterium-specific PCR primers that amplify genes coding for bacterial 16S rRNA.  
905 *Appl. Environ. Microbiol.* **64**: 795–799. doi:10.1128/aem.64.2.795-799.1998

906 McKnight, D. M., E. W. Boyer, P. K. Westerhoff, P. T. Doran, T. Kulbe, and D. T. Andersen. 2001.  
907 Spectrofluorometric characterization of dissolved organic matter for indication of precursor organic material  
908 and aromaticity. *Limnol. Oceanogr.* **46**: 38–48. doi:10.4319/lo.2001.46.1.0038

909 Montserrat, F., C. Van Colen, P. Provoost, M. Milla, M. Ponti, K. Van den Meersche, T. Ysebaert, and P. M. J.  
910 Herman. 2009. Sediment segregation by biodiffusing bivalves. *Estuar. Coast. Shelf Sci.* **83**: 379–391.  
911 doi:10.1016/j.ecss.2009.04.010

912 Morelle, J., P. Claquin, and F. Orvain. 2020. Evidence for better microphytobenthos dynamics in mixed sand/mud  
913 zones than in pure sand or mud intertidal flats (Seine estuary, Normandy, France). *PLoS One* **15**: e0237211.  
914 doi:10.1371/journal.pone.0237211

915 Morelle, J., O. Maire, A. Richard, A. Slimani, and F. Orvain. 2021. Contrasted impact of two macrofaunal species  
916 (*Hediste diversicolor* and *Scrobicularia plana*) on microphytobenthos spatial distribution and photosynthetic  
917 activity at microscale. *Mar. Environ. Res.* **163**. doi:10.1016/j.marenvres.2020.105228

918 Morelle, J., C. Roose-Amsaleg, and A. M. Laverman. 2022. Microphytobenthos as a source of labile organic matter  
919 for denitrifying microbes. *Estuar. Coast. Shelf Sci.* **275**. doi:10.1016/j.ecss.2022.108006

920 Morelle, J., M. Schapira, F. Orvain, and others. 2018. Annual Phytoplankton Primary Production Estimation in a  
921 Temperate Estuary by Coupling PAM and Carbon Incorporation Methods. *Estuaries and Coasts* 1–19.  
922 doi:10.1007/s12237-018-0369-8

923 Morgan-Kiss, R. M., J. C. Priscu, T. Pockock, L. Gudynaite-Savitch, and N. P. A. Huner. 2006. Adaptation and  
924 Acclimation of Photosynthetic Microorganisms to Permanently Cold Environments. *Microbiol. Mol. Biol.*  
925 *Rev.* **70**: 222–252. doi:10.1128/MMBR.70.1.222-252.2006

926 Muyzer, G., E. C. De Waal, and A. G. Uitterlinden. 1993. Profiling of complex microbial populations by  
927 denaturing gradient gel electrophoresis analysis of polymerase chain reaction-amplified genes coding for  
928 16S rRNA. *Appl. Environ. Microbiol.* **59**: 695–700. doi:10.1128/aem.59.3.695-700.1993

929 Oleszczuk, B., E. Michaud, N. Morata, P. E. Renaud, and M. Kędra. 2019. Benthic macrofaunal bioturbation  
930 activities from shelf to deep basin in spring to summer transition in the Arctic Ocean. *Mar. Environ. Res.*  
931 **150**: 104746. doi:10.1016/j.marenvres.2019.06.008

932 Orvain, F. 2005. A model of sediment transport under the influence of surface bioturbation: Generalisation to the  
933 facultative suspension-feeder *Scrobicularia plana*. *Mar. Ecol. Prog. Ser.* **286**: 43–56.

934 doi:10.3354/meps286043

935 Orvain, F., M. De Crignis, K. Guizien, S. Lefebvre, C. Mallet, E. Takahashi, and C. Dupuy. 2014. Tidal and  
936 seasonal effects on the short-term temporal patterns of bacteria, microphytobenthos and exopolymers in  
937 natural intertidal biofilms (Brouage, France). *J. Sea Res.*

938 Orvain, F., S. Lefebvre, J. Montepini, M. Sébire, A. Gangnery, and B. Sylvand. 2012. Spatial and temporal  
939 interaction between sediment and microphytobenthos in a temperate estuarine macro-intertidal bay. *Mar.*  
940 *Ecol. Prog. Ser.* **458**: 53–68.

941 Orvain, F., P. G. Sauriau, A. Sygut, L. Joassard, and P. Le Hir. 2004. Interacting effects of *Hydrobia ulvae*  
942 bioturbation and microphytobenthos on the erodibility of mudflat sediments. *Mar. Ecol. Prog. Ser.* **278**: 205–  
943 223. doi:10.3354/meps278205

944 Parlanti, E., K. Wörz, L. Geoffroy, and M. Lamotte. 2000. Dissolved organic matter fluorescence spectroscopy as  
945 a tool to estimate biological activity in a coastal zone submitted to anthropogenic inputs. *Org. Geochem.* **31**:  
946 1765–1781. doi:10.1016/S0146-6380(00)00124-8

947 Passarelli, C., C. Hubas, A. N. Segui, J. Grange, and T. Meziane. 2012. Surface adhesion of microphytobenthic  
948 biofilms is enhanced under *Hediste diversicolor* (O.F. Müller) trophic pressure. *J. Exp. Mar. Bio. Ecol.* **438**:  
949 52–60. doi:10.1016/j.jembe.2012.10.005

950 Paterson, D. M., I. Fortune, R. J. Aspden, and K. S. Black. 2019. Intertidal Flats: Form and Function, p. 383–406.  
951 *In Coastal Wetlands*. Elsevier.

952 Perkins, A. K., I. R. Santos, A. L. Rose, K. G. Schulz, H. P. Grossart, B. D. Eyre, B. P. Kelaher, and J. M. Oakes.  
953 2022. Production of dissolved carbon and alkalinity during macroalgal wrack degradation on beaches: a  
954 mesocosm experiment with implications for blue carbon. *Biogeochemistry* **160**: 159–175.  
955 doi:10.1007/s10533-022-00946-4

956 Pischedda, L., P. Cuny, J. L. Esteves, J. C. Poggiale, and F. Gilbert. 2012. Spatial oxygen heterogeneity in a  
957 *Hediste diversicolor* irrigated burrow. *Hydrobiologia* **680**: 109–124. doi:10.1007/s10750-011-0907-x

958 Quaiser, A., X. Bodi, A. Dufresne, and others. 2014. Unraveling the stratification of an iron-oxidizing microbial  
959 mat by metatranscriptomics. *PLoS One* **9**: 1–9. doi:10.1371/journal.pone.0102561

960 Raven, J., and R. J. Geider. 1988. Temperature and algal growth. *New Phytol.* **110**: 441–461. doi:10.1111/j.1469-  
961 8137.1988.tb00282.x

962 Redzuan, N. S., and G. J. C. Underwood. 2021. The importance of weather and tides on the resuspension and  
963 deposition of microphytobenthos (MPB) on intertidal mudflats. *Estuar. Coast. Shelf Sci.* **251**.  
964 doi:10.1016/j.ecss.2021.107190

965 Richard, A., F. Orvain, J. Morelle, and others. 2023. Impact of Sediment Bioturbation on Microphytobenthic  
966 Primary Producers: Importance of Macrobenthic Functional Traits. *Ecosystems* **26**: 1077–1094.  
967 doi:10.1007/s10021-022-00817-x

968 Riisgard, H. U. 1991a. Suspension feeding in the polychaete *Nereis diversicolor*. *Mar. Ecol. Prog. Ser.* **70**: 29–37.  
969 doi:10.3354/meps070029

970 Riisgard, H. U. 1991b. Suspension feeding in the polychaete *Nereis diversicolor*. *Mar. Ecol. Prog. Ser.* **70**: 29–37.  
971 doi:10.3354/meps070029

972 Riisgård, H., A. Vedel, H. Boye, and P. Larsen. 1992. Filter-net structure and pumping activity in the polychaete  
973 *Nereis diversicolor*: effects of temperature and pump-modelling. *Mar. Ecol. Prog. Ser.* **83**: 79–89.

974 doi:10.3354/meps083079  
975 Santos, S., P. C. Luttikhuisen, J. Campos, C. H. R. Heip, and H. W. van der Veer. 2011. Spatial distribution  
976 patterns of the peppery furrow shell *Scrobicularia plana* (da Costa, 1778) along the European coast: A  
977 review. *J. Sea Res.* **66**: 238–247. doi:10.1016/j.seares.2011.07.001  
978 Sanz-Lázaro, C., T. Valdemarsen, A. Marín, and M. Holmer. 2011. Effect of temperature on biogeochemistry of  
979 marine organic-enriched systems: Implications in a global warming scenario. *Ecol. Appl.* **21**: 2664–2677.  
980 doi:10.1890/10-2219.1  
981 Scaps, P. 2002. A review of the biology, ecology and potential use of the common ragworm *Hediste diversicolor*  
982 (O.F. Müller) (Annelida: Polychaeta). *Hydrobiologia* **470**: 203–218.  
983 Seeberg-Elverfeldt, J., M. Schlüter, T. Feseker, and M. Kölling. 2005. Rhizon sampling of porewaters near the  
984 sediment-water interface of aquatic systems. *Limnol. Oceanogr. Methods* **3**: 361–371.  
985 doi:10.4319/lom.2005.3.361  
986 Serôdio, J., S. Vieira, and F. Barroso. 2007. Relationship of variable chlorophyll fluorescence indices to  
987 photosynthetic rates in microphytobenthos. *Aquat. Microb. Ecol.* **49**: 71–85. doi:10.3354/ame01129  
988 Shen, Q., F. Ji, J. Wei, D. Fang, Q. Zhang, L. Jiang, A. Cai, and L. Kuang. 2020. The influence mechanism of  
989 temperature on solid phase denitrification based on denitrification performance, carbon balance, and  
990 microbial analysis. *Sci. Total Environ.* **732**. doi:10.1016/j.scitotenv.2020.139333  
991 Shen, Z., J. Hu, J. Wang, and Y. Zhou. 2015. Biological denitrification using starch/polycaprolactone blends as  
992 carbon source and biofilm support. *Desalin. Water Treat.* **54**: 609–615. doi:10.1080/19443994.2014.885395  
993 Stal, L. J. 2010. Microphytobenthos as a biogeomorphological force in intertidal sediment stabilization. *Ecol. Eng.*  
994 **36**: 236–245. doi:10.1016/j.ecoleng.2008.12.032  
995 Stal, L. J., and J. F. C. de Brouwer. 2003. Biofilm formation by benthic diatoms and their influence on the  
996 stabilization of intertidal mudflats. *Berichte – Forschungszentrum Terramare* **12**: 109–111.  
997 Swanberg, I. L. 1991. The influence of the filter-feeding bivalve *Cerastoderma edule* L. on microphytobenthos :  
998 a laboratory study. *J. Exp. Mar. Bio. Ecol.* **151**: 93–111.  
999 Takai, K., and K. Horikoshi. 2000. Rapid detection and quantification of members of the archaeal community by  
1000 quantitative PCR using fluorogenic probes. *Appl. Environ. Microbiol.* **66**: 5066–5072.  
1001 doi:10.1128/AEM.66.11.5066-5072.2000  
1002 Taylor, J. D., B. A. McKew, A. Kuhl, T. J. McGenity, and G. J. C. Underwood. 2013. Microphytobenthic  
1003 extracellular polymeric substances (EPS) in intertidal sediments fuel both generalist specialist EPS-  
1004 degrading bacteria. *Limnol. Oceanogr.* **58**: 1463–1480. doi:10.4319/lo.2013.58.4.1463  
1005 Thibault, A., S. Derenne, E. Parlanti, and others. 2019. Dynamics of organic matter in the Seine Estuary (France):  
1006 Bulk and structural approaches. *Mar. Chem.* **212**: 108–119. doi:10.1016/j.marchem.2019.04.007  
1007 Ubertini, M., S. Lefebvre, A. Gangnery, K. Grangeré, R. Le Gendre, and F. Orvain. 2012. Spatial variability of  
1008 benthic-pelagic coupling in an estuary ecosystem: consequences for microphytobenthos resuspension  
1009 phenomenon. *PLoS One* **7**: e44155. doi:10.1371/journal.pone.0044155  
1010 Underwood, G. J. C. 1994. Seasonal and spatial variation in epipellic diatom assemblages in the severn estuary.  
1011 *Diatom Res.* **9**: 451–472. doi:10.1080/0269249X.1994.9705319  
1012 Underwood, G. J. C., and J. C. Kromkamp. 1999. Primary Production by Phytoplankton and Microphytobenthos  
1013 in Estuaries. *Adv. Ecol. Res.* **29**: 93–153. doi:10.1016/S0065-2504(08)60192-0

- 1014 Vedel, A. 1998. Phytoplankton depletion in the benthic boundary layer caused by suspension-feeding *Nereis*  
1015 *diversicolor* (Polychaeta): grazing impact and effect of temperature. *Mar. Ecol. Prog. Ser.* **171**: 125–132.  
1016 doi:10.3354/meps171125
- 1017 Vonk, J. E., B. E. van Dongen, and Ö. Gustafsson. 2008. Lipid biomarker investigation of the origin and diagenetic  
1018 state of sub-arctic terrestrial organic matter presently exported into the northern Bothnian Bay. *Mar. Chem.*  
1019 **112**: 1–10. doi:10.1016/j.marchem.2008.07.001
- 1020 Weerman, E. J., P. M. J. Herman, and J. Van De Koppel. 2011. Macrobenthos abundance and distribution on a  
1021 spatially patterned intertidal flat. *Mar. Ecol. Prog. Ser.* **440**: 95–103. doi:10.3354/meps09332
- 1022 Widdows, J., A. Blauw, C. H. R. Heip, and others. 2004. Role of physical and biological processes in sediment  
1023 dynamics of a tidal flat in Westerschelde Estuary, SW Netherlands. *Mar. Ecol. Prog. Ser.* **274**: 41–56.
- 1024 Wiesebron, L. E., N. Steiner, C. Morys, T. Ysebaert, and T. J. Bouma. 2021. Sediment Bulk Density Effects on  
1025 Benthic Macrofauna Burrowing and Bioturbation Behavior. *Front. Mar. Sci.* **8**: 1–16.  
1026 doi:10.3389/fmars.2021.707785
- 1027 Wolff, W. J. 1973. The estuary as a habitat: an analysis of data on the soft-bottom macrofauna of the estuarine  
1028 area of the rivers Rhine, Meuse and Scheldt. *Zool. Verkan.* **126**: 1–242.
- 1029 Yallop, M. L., D. M. Paterson, and P. Wellsbury. 2000. Interrelationships between rates of microbial production,  
1030 exopolymer production, microbial biomass, and sediment stability in biofilms of intertidal sediments.  
1031 *Microb. Ecol.* **39**: 116–127. doi:10.1007/s002489900186
- 1032 Zhang, Y., J. Wang, J. Tao, and others. 2022. Concentrations of dissolved organic matter and methane in lakes in  
1033 Southwest China: Different roles of external factors and in-lake biota. *Water Res.* **225**: 119190.  
1034 doi:10.1016/j.watres.2022.119190
- 1035 Zsolnay, A., E. Baigar, M. Jimenez, B. Steinweg, and F. Saccomandi. 1999. Differentiating with fluorescence  
1036 spectroscopy the sources of dissolved organic matter in soils subjected to drying. *Chemosphere* **38**: 45–50.  
1037 doi:10.1016/S0045-6535(98)00166-0
- 1038 Zwarts, L., A.-M. Blomert, P. Spaak, and B. De Vriers. 1994. Feeding radius, burying depth and siphon size of  
1039 *Macoma balthica* and *Scrobicularia plana*. *J. Exp. Bot.* **183**: 193–212.
- 1040